Ca isotope cycling in a forested ecosystem

Chris Holmden[1] and Nicolas Bélanger[2]

Saskatchewan Isotope Laboratory[1], Department of Geological Sciences, University of Saskatchewan, 114 Science Place, Saskatoon, Saskatchewan, S7N 5E2. chris.holmden@usask.ca.

UER Sciences et technologies[2], Téluq, Université du Québec à Montréal, 100 Sherbrooke Ouest, Montréal, Québec, H2X 3P2. belanger.nicolas@teluq.uqam.ca.

ABSTRACT

Reports of large Ca isotope fractionations between trees and soils prompted this study of a Boreal forest ecosystem near La Ronge, Saskatchewan, to improve understanding of this phenomenon. The results on five tree species (black spruce, trembling aspen, white spruce, jack pine, balsam poplar) confirm that nutrient Ca uptake by plants favors the light isotopes, thus driving residual Ca in plant available soil pools towards enrichment in the heavy isotopes. Substantial within-tree fraction occurs in tissues formed along the transpiration stream, with low δ^{44}Ca values in fine roots (2mm), intermediate values in stemwood, and high values in foliage. Separation factors between different plant tissues are similar between species, but the initial fractionation step in the tips of the fine roots is species specific, and/or sensitive to the local soil environment. Soil water δ^{44}Ca values appear to increase with depth to at least 35 cm below the top of the forest floor, which is close to the deepest level of fine roots. The heavy plant fractionated signature of Ca in the finely rooted upper soils filters downward where it is retained on ion exchange sites, leached into groundwater, and discharged into surface waters.

The relationship between Ca uptake by tree fine roots and the pattern of ^{44}Ca enrichment with soil depth was modeled for two Ca pools: the forest floor (litter) and the underlying (upper B) mineral soil. Six study plots were investigated along two hillside toposequences trending upwards from a first order stream. We used allometric equations describing the Ca distribution in boreal tree species to calculate weighted average δ^{44}Ca values for the stands in each plot and estimate Ca uptake rates. The δ^{44}Ca value of precipitation was measured, and soil weathering signatures deduced, by acid leaching of lower B mineral soils. Steady state equations were used to derive a set of model Ca fluxes and fractionation factors for each plot. The model reproduces the increase in δ^{44}Ca with depth found in forest floor and upper B soil waters. Transient model runs show that the forest Ca cycle is sensitive to changes in plant Ca uptake rate, such as would occur during ontogeny or disturbance. Accordingly, secular records of δ^{44}Ca in tree ring cellulose have the potential to monitor changes in the forest Ca cycle through time, thus providing a new

tool for evaluating natural and anthropogenic impacts on forest health. Another model run shows that by changing the size of the isotope fractionation factor and adjusting for differences in forest productivity, that the range in Ca isotope fractionation in forested ecosystems reported in the literature, thus far, is reproduced. As a quantitative tool, the Ca cycling model produces a reasonable set of relative Ca fluxes for the La Ronge site, consistent with Environment Canada's measurements for wet deposition in the region and simulated Ca release from soil mineral weathering using the PROFILE model. But the sensitivity of the model is limited by the small range of fractionation observed in this boreal shield setting of ~1‰, which limits accuracy. If the model were applied to a site with a greater range in $\delta^{44}Ca$ values among the principal Ca fluxes, it is capable of producing robust and reliable estimations of Ca fluxes that are otherwise difficult to measure in forested ecosystems.

1. INTRODUCTION

Biogeochemical cycling of Ca in forest ecosystems causes fractionation of Ca isotopes. The ~4‰ range of fractionation documented, thus far, (Schmitt et al., 2003; Bullen et al., 2004; Wiegand et al., 2005; Holmden and Bélanger, 2006; Perakis et al., 2006; Page et al., 2008; Cenki Tok et al., 2009) is much larger than the ~1‰ effects associated with biotic (Russell and Papanastassiou, 1978a; Skulan et al., 1997; Zhu and MacDougall, 1998; Gussone et al., 2003; Sime et al., 2005; Steuber and Buhl, 2006; Fantle and DePaolo, 2005; Farkas et al., 2007) and abiotic (Lemarchand et al., 2004; Gussone et al., 2005; Fantle and DePaolo, 2007; Jacobson and Holmden, 2008; Ewing et al., 2008) precipitation of Ca bearing minerals from natural waters, or the small range of Ca isotope fractionation in rocks of the crust and upper mantle of about the same magnitude (DePaolo et al., 2004; Amini et al., 2008). These findings point to vegetation and soils as potentially important sources of isotopically fractionated Ca in the Earth's exogenic Ca cycle.

The uptake of Ca into trees favors the lighter isotopes, which causes the residual Ca in soil exchange pools to accumulate the heavier isotopes. Fractionation of Ca isotopes also occurs

between different tissues in trees. For example, Ca in stemwood is depleted in heavy isotopes compared to foliage, but both are enriched in light isotopes compared to plant available soil pools (Holmden and Bélanger, 2006; Page et al., 2008; Cenki Tok et al., 2009). The underlying physiological mechanisms, the prevalence of species effects, and the range of environmental controls that may influence Ca isotope fractionation in trees are not well known.

To improve our understanding of isotope fractionation effects accompanying Ca cycling in forests, we studied an unpolluted Boreal Shield watershed in northern Saskatchewan that was recently the subject of a Ca apportionment study to trees using $^{87}Sr/^{86}Sr$ as a tracer (Bélanger and Holmden, submitted). Measurements of $\delta^{44}Ca$ in foliage, stemwood, and fine roots were performed on 5 tree species typical of this ecosystem, growing on a small hillside watershed with a first order stream. The $\delta^{44}Ca$ values in soil solutions, soil extracts, soil leaches, shallow groundwater, granite bedrock, precipitation, and stream waters were also measured, thus, generating a complete survey of $\delta^{44}Ca$ variability in a high latitude terrestrial ecosystem. We investigate the factors controlling $\delta^{44}Ca$ values in plant available soil pools with the help of a steady state Ca cycling model, and an allometric analysis of the Ca distribution in trees. The model is employed to produce a set of balanced Ca fluxes and plant uptake fractionation factors for six study plots differing in soil texture, soil mineralogy, elevation, and stand composition.

2. STUDY SITE AND EXPERIMENTAL DESIGN

2.1 Study site and design

The study site is a hillside watershed with a first order stream, located along the southern edge of the Precambrian Shield in north-central Saskatchewan, ~40 km north of the town of La Ronge (55° 6' 0" N, 105° 18' 0" W), and ~400 km north of Saskatoon (Fig. 1). Mean annual air temperature is –0.1ºC and precipitation is 484 mm. The forests are black spruce/trembling aspen

89 stands with subsidiary amounts of jack pine. Dendrochronological analysis of the trees revealed
90 two cohorts: one with an age of 80–90 years on slopes and hilltops, and another with an age of
91 110–120 years in the flood plain of the stream. The forest has never been harvested, and it is
92 presumed that the ages reflect the last time the forest was destroyed by fire. Burn cycles of ~100
93 years are typical in this region. In 2006, a major fire burned thousands of hectares of forest near
94 La Ronge, but the area surrounding the studied watershed was left intact (Saskatchewan
95 Environment, 2006).

96 The study site was broken up into three 75 m^2 circular plots strung along two hillside
97 toposequences. Plots in Toposequence 1 are identified as 1.1, 1.2, and 1.3 (Fig. 2). Plot 1.1 covers
98 the highest parts of the slope, plot 1.2 covers the midslope, and plot 1.3 covers the lowermost
99 slope and riparian zone. Toposequence 2 covers two drainage valleys. Plots identified as 2.2 and
100 2.3 are from the same hillside, and cover the same range of elevations as Toposequence 1, about
101 40 m upstream (Fig. 3). Plot 2.1 covers a shallow, bowl-like depression at the top of the hill that
102 gently slopes towards the next valley. It lies about 3 m below the top of Toposequence 1. The
103 middle and upper slopes of Toposequence 1 (where the soils are sandier and better drained) range
104 into mixed wood forests with spruce, trembling aspen, and some jack pine. In areas near the
105 stream where the water table is high throughout the growing season (20 to 40 cm depth), balsam
106 poplar and white spruce are found alongside the dominant black spruce. The forest on
107 Toposequence 2 is uniformly black spruce with a feathermoss understory.

108 General soil properties are tabulated in Bélanger and Holmden (submitted). Soils under
109 the mixedwood vary from sandy loam to loam in the upper slope areas, and to silt loam in the
110 mid-slope areas. The soils under the black spruce/feathermoss are sandy loam to silt loam at mid-
111 slope, and silt loam to silty clay at the top. These are, respectively, Eluviated Dystric Brunisols
112 and Orthic Eutric Brunisols (Expert Committee on Soil Survey, 1998). Soils at the bottom of the
113 hill and in the riparian zone are silt loam to heavy clay and are classified as Orthic Gleysols or

Orthic Humic Gleysols. The forest floor is generally a mor-moder humus form for the Brunisols and a moder for the Gleysols.

Zero-tension lysimeters were installed in each plot below the forest floor (10 cm) and at a depth of 25 cm in the mineral soil (MacDonald et al., 2007). In the riparian plots, porous cup tension lysimeters (Soil Moisture Equipment, Santa Barbara, CA) were installed at depths of 10 and 25 cm in the mineral soil. Shallow groundwater was monitored with 30 cm PVC piezometers screened at depths of 1.4 and 1.8 m. The first four sets of soil solution and shallow groundwater samples (June 23 and 30, and July 6 and 14) were discarded and then re-sampled on July 30, August 31, September 21, and October 20. All isotopic analyses were performed on the samples collected on September 21, 2005, as all collectors yielded a sample.

Rainwater was collected throughout the growing season as wet-only deposition using an automated and chemically clean wet-only deposition collector (Model 200, Ecotech, Blackburn, Australia). The collector was installed on top of a 14 m high aircraft hangar that is used by the forest fire fighting crew just outside the town of La Ronge. In addition, snow cores were collected from Lac La Ronge (55° 6' 0 N; 105° 17' 60 W) and lake Nemeiben (55° 19' 60 N; 105° 19' 60 W) in March 2005, approximately 500 m from shore to avoid contamination by vegetation debris in order to obtain the best possible regional atmospheric signal. High density 20 L acid-washed polyethylene pails and lids were pre-contaminated with the snow from each lake, and snow samples were collected by driving down several times into the snow pack. The snow samples were thawed within hours of collection and ~250 ml of the melt water was transferred into pre-cleaned polyethylene bottles.

Foliage and stemwood were sampled on August 31 from one dominant or co-dominant tree, and one understory (young) tree when present, of each species in each plot. Foliage exposed to direct sunlight (located in the upper half of the canopy) was targeted and sampled using a shotgun. No attempt was made to separate foliage into age classes. Stemwood was sampled at 1.3 m from the ground using a 4.1 mm-diameter Haglöf® increment borer.

In addition to the field study, an aspen seedling was grown *in vivo* on crushed basalt (very fine sand and silt) mixed with pure quartz (fine sand) at a weight ratio of 15:1. Before planting, seed stratification was performed by soaking the seeds in a mix of water and pure quartz sand for one week. Seedlings were grown for 6 weeks in a growing chamber set at 21°C and 40% air humidity with 15 hours of sunlight per day. A Hoagland-type nutrient solution was used to feed the seedlings, except that it was Ca free. It was added every 2 to 3 days, keeping the surface soil moist to the touch. The seedling was harvested after two months of growth, and aliquots of leaf, stem, root radicle, and fine root were sampled for analysis.

3. ANALYTICAL METHODS

3.1 Ca pools in soils and trees

Forest floor bulk density was obtained by cutting around a 20 cm × 20 cm template (slash, litter layer, moss cover, and large roots removed) and then measuring its depth and oven-dry mass. Bulk density of upper mineral soil was also assessed on oven-dried samples after sampling the soil with a bucket auger with a known volume (0-20 cm and 20-40 cm increments). The discontinuous Ae horizon of the Eluviated Dystric Brunisols (mixedwood) was not sampled because it is difficult to separate it from the forest floor and mineral soil in this setting. The product of soil bulk density and exchangeable Ca concentration was used to estimate the size of soil exchangeable Ca pools.

Allometric equations developed by Lambert et al. (2005) were employed to estimate the aboveground biomass density (organic dry mass per unit area) in each plot (Bélanger and Holmden, submitted). Stem, bark, branches, and canopy biomass were assessed individually for each species using the diameter at breast height data as input. Total aboveground Ca content in each plot was estimated as the sum of Ca content in stemwood, bark, foliage, and branches. Root biomass, not part of Lambert's equations, was estimated using above and below ground biomass

data collected on boreal species near Candle Lake, Saskatchewan (Kalyn and Van Rees, 2006). The root biomass fractions were calculated for black and white spruce, aspen, and jack pine, and applied to the La Ronge stands to estimate root biomass in each plot. The Ca content of root biomass was calculated using the Ca concentrations for branches given by Lambert et al. (2005). Branches are higher in Ca than stemwood and lower than foliage. Taking this approach, the roots added 10–20% more Ca to the vegetation pools in each study plot.

3.2 Sample digests and Ca concentrations

All solutions were filtered through 0.4 μm polycarbonate membranes in a Class 10,000 trace metal clean room in the Saskatchewan Isotope Laboratory. Foliage and stemwood samples were oven-dried for 48 h at 65ºC. Root samples were cleared of soil particles by repeated rinsing and sonication in ultra pure water, and checked for cleanliness using a binocular microscope. No adhering particles were observed. The dried samples were then broken up and digested in ultrapure ~15 N HNO_3 using 150 to 500 ml PTFE beakers covered with PTFE 'watch glasses' on a hot plate at 130ºC for 3 days.

One gram samples of lower B horizon mineral soil from each plot were extracted with 10 ml of 0.1 N $BaCl_2$ solution (purity 99.999%) on a shaker for 2 hours. This served as a proxy for exchangeable cations, including Ca and Sr. The sample was rinsed and decanted several times with ultrapure water to remove excess $BaCl_2$ and then subjected to a weak acid leach using 1 N HNO_3 at room temperature for 2 hours. According to Nezat et al. (2007), this weak digest removes Ca and Sr from the crystal lattice of apatite and possibly some Ca and Sr contained in biotite and chlorite. The supernate was removed by centrifugation and the residue treated with 10 ml of 15 N HNO_3 for 8 hours at 70ºC. The supernate was again removed, and an aliquot of the remaining sample digested in HF-HNO_3. The HF-HNO_3 digests remove Ca and Sr held in the more refractory minerals such as muscovite, alkali feldspar, and plagioclase (Nezat et al. 2007). A finely ground sample of the local granite was also subjected to the 1 N and 15 N HNO_3 digests,

and another sample was dissolved completely in HF-HNO_3. Calcium concentrations for all samples were measured by isotope dilution thermal ionization mass spectrometry (ID-TIMS).

3.3 $\delta^{44}Ca$ measurements

Aliquots of clear solutions corresponding to 50 μg of Ca were mixed with aliquots of ^{43}Ca-^{42}Ca double spike to achieve a target mixed $^{40}Ca/^{42}Ca$ ratio of 7.0. The solution was then dried down, resolublized, and dried down again to promote equilibration of spike and sample isotopes. This step is performed before the samples are loaded onto the ion exchange columns. This ensures that any isotope fractionation that may occur on the columns, from yields that are less than 100%, is corrected for at the same time as the mass discrimination correction for fractionation in the mass spectrometer. The preparation and composition of the double spike is given in Holmden (2005). Calcium is purified from K and Sr using Teflon columns from Savillex® filled with 3 ml of Biorad® MP50 cation exchange resin. To minimize blank, all sample containers and pipettes were cleaned in 2 N HNO_3 and thoroughly rinsed in ultrapure water. Tests showed that most of the Ca blank originated from the columns and loading. The total combined column and loading blank was controlled to between 80 and 130 ng, measured by isotope dilution. The Ca blank has a 'normal' isotopic composition ($\delta^{44}Ca$ = –1.27‰) typical of the values measured in terrestrial samples. At a sample to blank ratio of 500 the blank contribution is negligible, and no correction for blank contribution was applied to the data. After the pure Ca aliquot was dried, two drops of H_2O_2 were added and dried to help oxidize organics contributed from the column, followed by 2 drops of 15 N HNO_3 to convert the sample to the nitrate form for loading.

Loading was performed under a binocular microscope using a 0.5–10 μl range digital pipette. Between 3 and 8 μg of Ca was loaded onto single, out-gassed Ta filaments (0.00137"

thick, 0.030" wide) using parafilm dams to limit the spread of the sample. Between 0.5 and 1.0 ml of 10% ultrapure H_3PO_4 was then added to the load and the solution dried, carefully, by raising the filament current. The sample does not dry completely because water is absorbed from the air as the filament current is increased. The parafilm melts, and the sample eventually boils as moisture escapes from the viscous load. The current is increased further, and boiling is allowed to continue for one or two minutes to homogenize the load, and possibly allow Ta from the filament to dissolve and mix into the load. Tantalum is known to increase Ca ionization efficiency in the mass spectrometer.

In the mass spectrometer, the filament current is increased slowly over a period of about 40 minutes until a ^{44}Ca ion beam of ~50 mV is achieved (10^{11} ohm resistor). At this point, or shortly thereafter, the ion beam intensities will increase with little or no additional increase in the filament current. Often times it will be necessary to lower the current in order to slow the rapidly increasing ion beam currents. During a run, however, the beam growth is restricted to 5%, and is checked between blocks. Initially, focusing is performed semi-automatically (i.e., with operator oversight) with the goal of maximizing the ion beam intensities and perfecting peak shape, and then by computer control once every five blocks during the run. The Ca isotope measurements are performed in three scans (or hops) of the magnetic field to restrict the mass range of the measurements to 5% in order to minimize potential ion optical effects (Fletcher et al., 1997; Holmden, 2005; and Appendix A for further details). Data collection begins when the ^{44}Ca ion beam intensity is between 200 and 400 mV, with corresponding ^{40}Ca intensities between 10 and 20 V. Typically, data representing 18 blocks of ten cycles each are collected. Each cycle takes 43 seconds to complete, with 30-second baselines between cycles, for a total run time of about three hours. The reason for the long analysis is to provide a sufficient record of the behavior of the run so as to confidently assess its quality, although ion-counting statistics are also improved. High quality runs show: (1) no shift in mass bias corrected ratios after focusing, (2) no drift in mass bias corrected ratios with time, and (3) a normal and steady fractionation trend with time showing

241 increased heavy isotope enrichment of residual Ca on the filament. Any periods of reverse
242 fractionation, or runs characterized by erratic patterns of fractionation, signify that the Ca on the
243 filament may be parceled into multiple reservoirs, each fractionating at different rates (e.g., Hart
244 and Zindler, 1989; Upadhyay et al., 2008; Fantle and Bullen et al., 2009). This type of
245 evaporation and ionization behavior on the filament greatly degrades the effectiveness of the
246 instrumental mass bias correction and the accuracy of the data. When beam growth and isotopic
247 fractionation are steady throughout a long run, it implies that Ca is being drawn from a single
248 homogenous reservoir on the filament.

249 Three ratios are constructed from the collected data: (1) $^{40}Ca/^{42}Ca$ from the first hop, (2)
250 $^{42}Ca/^{43}Ca$ from the second hop, and (3) $^{42}Ca/^{44}Ca$ from the combined second and third hops.
251 $^{41}K/^{42}Ca$ is monitored in the first hop, but the ratio is so low that corrections for ^{40}K interference
252 on ^{40}Ca are never required (see Appendix A for collector configuration). The mixed composition
253 runs are corrected for instrumental mass bias, and the tracer Ca unmixed from the sample, using
254 equations published in Eugster et al. (1969), which are solved iteratively in a spreadsheet.
255 Calcium isotopic data are reported in the standard delta (δ) notation as variations in $^{44}Ca/^{40}Ca$
256 relative to measurements of natural seawater. Pacific, North Atlantic, and Caribbean seawater
257 have been measured, and it is found that their $\delta^{44}Ca$ values are identical within the uncertainties
258 of the measurements, in agreement with (Hippler et al. 2003). Ultimately, the reproducibility of
259 the measurements is based on the analyst's ability to correct for instrumental drift (Appendix A)
260 and the care and attention being paid to loading, focusing, and fractionation during the run. For
261 these reasons we have not yet attempted to run a sequence of Ca samples under complete
262 computer control.

263 The reproducibility for a single, drift-corrected measurement of $\delta^{44}Ca$ is ±0.07‰ (2σ),
264 which is estimated by taking the standard deviation of 90 measurements of two internal standards:
265 41 CaF_2 and 49 seawater, from 24 measurement sessions (each one of approximately two weeks

duration) over the last, approximately, two years. Instrumental drift is corrected for by adjusting the isotope composition of the double spike in each measurement session (using an exponential law) to achieve an average isotopic difference of –1.29‰ between the two standards employed for this purpose ($\delta^{44}Ca_{CaF2} - \delta^{44}Ca_{seawater}$) (Appendix A). The drift corrected δ^{44}Ca value of 915a measured over the past two years is –1.86 ±0.05‰ (2σ, n=13).

4. FOREST FLOOR CALCIUM MODEL

A simple model that captures the impact of forest growth on the δ^{44}Ca values in plant available soil pools consists of two boxes (Fig. 4). The upper box is the exchangeable Ca pool of the forest floor (M_{FF}), which represents the litter layer of the forest floor of ~10 cm thickness. The lower box is the exchangeable Ca pool of the upper B horizon (M_B), which represents the mineral soil of ~25 cm thickness. The two pools are intended to cover the range of soil depths permeated by tree fine roots, which draw Ca from these pools to support forest growth. The definitions of the components and units employed are listed in Table 1.

The amount of Ca in each ion exchange pool (M_i) is given in units of mol m^{-2}, which takes into account the thickness of the pool. Moreover, each pool is considered to be isotopically homogenous in δ_i, and identical to the soil solutions that filtered through them into the lysimeters.

The arrows in Fig. 4 represent Ca fluxes. The principle input fluxes include soil mineral weathering (f_w), atmospheric deposition (f_a), and leach losses from litterfall (f_{lf}). The principle output fluxes include plant uptake (f_u), leach losses from the forest floor to the upper B soil mineral pool (f_z), and leach losses from upper B to groundwater (f_{gw}). The δ^{44}Ca values for fluxes f_a, f_w, f_{lf}, f_z, and f_{gw} are, respectively, δ_a, δ_w, δ_{lf}, δ_{FF}, and δ_B.

290 Equations 1.1–1.4 are the model's mass balance and isotope mass balance framework
291 equations.

292 $$\frac{dM_{FF}}{dt} = f_a + f_{lf} - \left[f_z + f_u X \right] \quad (1.1)$$

293 $$\frac{dM_B}{dt} = f_w + f_z - [f_u (1-X) + f_{gw}] \quad (1.2)$$

294 $$\frac{d(M_{FF}\delta_{FF})}{dt} = f_a \delta_a + f_{lf}\delta_{lf} - \left[f_u X(\delta_{FF} + \Delta_{soil}^{veg}) + f_z \delta_{FF} \right] \quad (1.3)$$

295 $$\frac{d(M_B\delta_B)}{dt} = f_z \delta_{FF} + f_w \delta_w - \left[f_u (1-X)(\delta_B + \Delta_{soil}^{veg}) + f_{gw}\delta_B \right] \quad (1.4)$$

296
297 A close examination of the equations, and Fig. 4, shows that the atmospheric Ca flux
298 enters the forest Ca cycle through the forest floor pool, whereas the soil mineral weathering Ca
299 flux enters through the upper B mineral soil pool. The fraction of Ca drawn into the trees from the
300 forest floor pool is X, and from the upper B pool $(1-X)$.

301 Fixed parameters include the measured δ^{44}Ca values in the soil (δ_{FF}, δ_B) and vegetation
302 pools (δ_{veg}), seasonally averaged precipitation (δ_a), soil mineral weathering (δ_w), and the Ca
303 uptake flux (f_u). The fractionation factor Δ_{soil}^{veg} ($=\delta_{veg} - \delta_{soil}$) is determined individually for each
304 study plot (see section 5.4).

305 To achieve a balanced model (all Ca fluxes positive), the value of f_a is adjusted until the
306 model derived proportions of Ca from atmospheric deposition and soil mineral weathering (mixed
307 and immobilized in the vegetation) match the Ca apportionment constraints deduced using the
308 ^{87}Sr/^{86}Sr technique (Miller et al., 1993; Chadwick et al., 1999; Kennedy et al., 1998; Kennedy et
309 al., 2002; Bullen and Bailey, 2005; Drouet et al., 2005; Bélanger and Holmden, submitted). A
310 second constraint is that 80% of the trees annualized Ca requirement is from recycled litterfall, a
311 fraction deduced by Miller et al. (1993) using the ^{87}Sr/^{86}Sr tracer technique in the Adirondacks of

New York State (see section 5.4 for further discussion). Steady state equations, such as Eq 1.5 for f_w, are used to calculate a set of Ca fluxes for f_{lf}, f_z, f_w, and f_{gw}.

$$f_w = \frac{f_a\left(\delta_{FF} - \delta_B\right) + f_{lf}\left(\delta_{FF} - \delta_B\right) + Xf_u\left(\delta_B + \Delta_{soil}^{veg} - \delta_{FF}\right) - f_u\,\Delta_{soil}^{veg}}{\left(\delta_B - \delta_w\right)} \qquad (1.5)$$

5. RESULTS

5.1 δ^{44}Ca in vegetation

Stemwood is ^{44}Ca-depleted relative to soil solutions and groundwater in the same plots at all depths (Figures 2, 3; Table 2). Foliage is ^{44}Ca-enriched relative to stemwood, indicating significant within-tree fractionation, but is ^{44}Ca-depleted relative to soil and groundwater Ca pools. Values of δ^{44}Ca in stemwood range between –1.14 and –1.75‰ for five species across the six study plots, whereas foliage values range between –0.64 and –1.46‰.

An aspen seedling grown *in vivo* on powdered basaltic rock (δ^{44}Ca = –0.88‰) showed strongly developed fractionation between the first leaves (–0.52‰) and stem (–1.38‰). The seedling's roots, both radicle (–1.30‰) and secondary (–1.29‰), were not significantly different from the stem. Fine root (2 mm) δ^{44}Ca values in mature trees from the La Ronge site are lower than stemwood values which, in turn, are lower than foliage values. A positive δ^{44}Ca gradient characterizes tissues formed along the transpiration stream (Wiegand et al., 2005; Holmden and Bélanger, 2006; Perakis et al., 2006; Page et al., 2008; Cenki Tok et al., 2009).

Separation factors offer a convenient way to gauge the extent of Ca isotope fractionation between different tree components and their respective soil pools (Table 3). There is a reasonably good 1:1 correlation between δ^{44}Ca in foliage and stemwood (Fig. 5), suggesting a robust and stable pattern of within-tree fractionation. Some of the scatter may be due to time averaging of possible secular trends in the δ^{44}Ca values of stemwood, which were sampled without regard for

336 the age of the sampled increment. By contrast, the foliage samples reflect current growth
337 (deciduous), or seven years of growth (conifer). The average separation factor between foliage
338 and stemwood measured over four plots and all tree species is 0.43 ±0.12‰ (Table 3). The same
339 average difference of 0.41 ±0.05‰ was found between stemwood and fine roots. The total
340 average fractionation from root tips to canopy in the La Ronge forest is 0.84‰, which is virtually
341 identical to the 0.77‰ fractionation documented for the aspen seedling grown *in vivo*. The
342 magnitude of within-tree fractionation of Ca isotopes between different tissues is similar among
343 the studied tree species.

344 By contrast, the fractionation of Ca isotopes between the above and below ground Ca
345 pools is about half the magnitude in jack pine compared to the other tree species. This finding is
346 robust as it was reproduced for jack pine from three different study plots (Table 3) with differing
347 soil pool δ^{44}Ca values. Accordingly, the initial fractionation step in fine root tips may vary among
348 species more widely than the internal isotope fractionation of Ca between different tree tissues.
349 We found no consistent difference in δ^{44}Ca values between foliage and stemwood from old (85–
350 110 y) *vs.* young (~10–40 y) trees—the average difference (old-young) being –0.03 ±0.1‰ (n=3,
351 1σ).

352

353 ## 5.2 δ^{44}Ca in soil pools, groundwater, and streamwater

354 Soil water δ^{44}Ca values collected using lysimeters emplaced at the base of the forest floor
355 (10 cm), selected Ah (20 cm), and upper B horizons (35 cm) are reported in Table 2 (numbers in
356 parentheses indicate depth from surface). The soil water δ^{44}Ca values are lower in the forest floor
357 and higher in the mineral soils for all plots (Figs. 2, 3). To test whether the increase in δ^{44}Ca with
358 depth continues below the level of the fine roots (>35 cm), Ca was extracted using a $BaCl_2$
359 solution from the lower B/C mineral soils at 50–65 cm depth. Although slight increases of
360 between 0.1 and 0.2‰ are observed in three study plots (1.3, 2.1, and 2.2), the average difference

361 in $\delta^{44}Ca$ value between lower B/C soil extracts and upper B soil waters from six plots is close to
362 zero (0.05 ±0.13‰, 1σ). This is consistent with groundwater samples collected from 1.4 and 1.8
363 m depths from the riparian plots (1.3 and 2.3), which yielded an average $\delta^{44}Ca$ value of –0.67
364 ±0.21‰. This is within the uncertainty of the upper B soil waters from the same plots (–0.63
365 ±0.25‰). These are in turn similar to eight streamwater samples collected at the base of
366 Toposequence 1 over the course of the 2005 season, which yielded an average $\delta^{44}Ca$ value of –
367 0.61 ±0.05‰ (1σ).
368
369 ## 5.3 $\delta^{44}Ca$ in bedrock, soil mineral weathering release, and atmospheric deposition
370 Wet-only deposition during the summer months was found to be lower in $\delta^{44}Ca$ (–1.31‰,
371 n=2) than winter precipitation sampled from snow pack on nearby Lac La Ronge and Nemeiben
372 Lakes (–1.22‰, n=3, excluding the lowest value in Table 2). From these $\delta^{44}Ca$ data a weighted
373 average value of –1.28‰ is calculated for a mixture of 30% snowmelt and 70% summer
374 precipitation.
375 A whole-rock HF-HNO_3 digest of the granite bedrock yielded a $\delta^{44}Ca$ value of –1.27‰,
376 which is virtually identical to the annualized $\delta^{44}Ca$ value in precipitation. Because Ca release
377 from granite weathering is non-stochiometric owing to differences in mineral solubilities, the
378 granite was powdered and leached sequentially with 1 N and 15 N HNO_3 solutions. The 15 N
379 acid leachate (–1.57‰) was lower in $\delta^{44}Ca$ than the totally digested whole-rock (–1.27‰) and the
380 1 N HNO_3 leachate (–1.36‰) (Table 2). This finding is consistent with the hypothesis of
381 preferential release of radiogenic ^{40}Ca from biotite dissolution, which is supported by the pattern
382 of ^{87}Sr release (Bélanger and Holmden, submitted) (Table 2).
383 To obtain a more realistic estimate of the $\delta^{44}Ca$ signature of soil mineral weathering,
384 samples from the lower B/C horizons in each study plot were subjected to weak and concentrated
385 HNO_3 acid leaches after first removing the exchangeable Ca ions using a 0.1 N $BaCl_2$ solution.

386 The results are listed in Table 2 and plotted in Fig. 6 against their corresponding $^{87}Sr/^{86}Sr$ ratios.
387 Although the sequential treatment yielded increasingly radiogenic $^{87}Sr/^{86}Sr$ ratios in the leachates,
388 the less negative $\delta^{44}Ca$ values indicate that a large fractionation of the co-released Ca bears the
389 heavy isotope signature of plant-induced fractionation. This means that a sizeable fraction of the
390 Ca and Sr in the leachates does not come from the weathering of pristine igneous minerals, but
391 rather, has filtered down from the upper B horizon and become trapped in secondary mineral
392 growth (e.g. interlayers of clays), and/or captured by (less exchangeable) ion exchange sites.
393 Taking a closer look at the trends in Fig. 6 reveals two 'plateau values' that further leaching will
394 unlikely change. The coarser textured soils of plots 1.1 and 1.2 reached –1.06 ±0.01‰. The other
395 four plots reached –1.16 ±0.02‰. This finding is consistent with the relatively small range of
396 $\delta^{44}Ca$ values among igneous minerals compared to the relatively large range in $^{87}Sr/^{86}Sr$. As a
397 case in point, during the leaching of the granite powder, $\delta^{44}Ca$ values decreased by just 0.3‰,
398 which reflects preferential dissolution of ^{40}Ca enriched biotite. By contrast, the corresponding
399 change in $^{87}Sr/^{86}Sr$ is 260‰ owing to the high levels of ^{87}Rb in biotite and the ~1.85 Ga age of the
400 granite.
401

402 ## 5.4 Plot specific vegetation–soil fractionation factors

403 The Ca isotope fractionation factor (Δ_{soil}^{veg}) is an important quantity that requires careful
404 consideration. The separation factors listed in Table 3 were calculated without taking into account
405 the isotope mass balance of Ca between different tree tissues. Calcium translocation in trees
406 causes isotopic fractionation of Ca, as evidenced from the differences in $\delta^{44}Ca$ values between
407 foliage and stemwood (Table 2). Yet, there must be a primary fractionation step that occurs in the
408 root tips of the fine roots because the $\delta^{44}Ca$ values of the soil pools are ^{44}Ca enriched (–0.45 to –
409 1.05‰) relative to Ca inputs from atmospheric deposition (–1.28‰), soil mineral weathering (–
410 1.06 to –1.16‰), and foliage (–1.15 to –1.36‰) the principal component of litterfall (Table 4).

411 The first step towards calculating a bulk fractionation factor for the stands in each plot is to
412 compute the δ^{44}Ca values of each tree species from the Ca mass fractions and δ^{44}Ca values of the
413 major tree tissues using the Ca allometry (Table 4), and then computing δ_{veg} by weighting whole-
414 tree δ^{44}Ca values for each species against the species biomass distribution in the plot (Table 4).

415 The soil pools present a different problem. A δ^{44}Ca value is needed that reflects the
416 impact of the Ca taken up by plants, so that the fractionation factor can be calculated by
417 difference ($\delta_{veg} - \delta_{soil}$). But trees draw Ca from pools in the forest floor and mineral soil, which
418 differ in their δ^{44}Ca values. Therefore, we cannot determine Δ_{soil}^{veg} without first considering how
419 the uptake of Ca into the trees is split between Ca pools in the forest floor (X) and upper B
420 mineral soil ($1-X$). This is done through the use of a simple mixing equation (Eq. 1.6) that
421 relates changes in Δ_{soil}^{veg} to X using measured values of δ_{veg}, δ_{FF}, and δ_B:

422 $$\Delta_{soil}^{veg} = (\delta_{veg} - \delta_B) - X(\delta_{FF} - \delta_B) \quad (1.6)$$

423 At the present time, we cannot determine Δ_{soil}^{veg} independently from X, thus, we employ
424 the steady state equations and trial values of Δ_{soil}^{veg} to calculate a trial set of model Ca fluxes for
425 each plot. These fluxes, in turn, are used to calculate two additional quantities: (1) the fraction of
426 Ca in vegetation that is derived from atmospheric deposition *vs.* soil mineral weathering, which
427 must match the Ca apportionment constraints deduced from the $^{87}Sr/^{86}Sr$ study (Bélanger and
428 Holmden, submitted), and (2) the fraction of the forest's annualized Ca requirement that is
429 internally cycled through litterfall, which we set at 80% of the total Ca inputs to the forest. The
430 value for Δ_{soil}^{veg} is adjusted until conditions (1) and (2) are satisfied. Taking this approach, the
431 average value of X is 0.64 ±0.12 (1σ), and the average value of Δ_{soil}^{veg} is –0.70 ±0.13 (1σ) (Table
432 5). How closely the model results approach the magnitudes of the true Ca fluxes depends on four
433 sources of uncertainty: (1) the degree to which the measured δ-values genuinely reflect the Ca

pools to which they are assigned, (2) the validity of the $^{87}Sr/^{86}Sr$ based study of Ca partitioning between atmospheric and soil mineral weathering sources in trees, (3) the appropriateness of the assumption that 80% of the annualized Ca input to the forest Ca cycle is from litterfall, and (4) the accuracy of the plant uptake Ca flux (f_u).

5.5 Model results

5.5.1 Steady state solutions

Forest growth rates are typically highest during the middle stage of development, which corresponds to important increments in stemwood volume (Miller, 1995). Since the La Ronge forest is mature, most of the trees' resources are presently directed towards maintaining the canopy; thus, its current growth rate is relatively low. Accordingly, the Ca uptake rate in the mature forest is broadly equivalent to the amount of Ca needed to support the annual turnover of foliage in the canopy, which may be deduced from the Ca allometry. It follows that we calculated the mass of Ca in the deciduous leaves (dividing by the average hang time of one year) and conifer needles (dividing by the average hang time of seven years) in each plot, and then summed the results to determine the annualized Ca uptake for each plot. Values of f_u scale positively with the values of f_a, f_w and f_{lf}, as dictated by the isotope mass balance constraints imposed by the measured $\delta^{44}Ca$ values in each soil pool. Consequently, if f_u is underestimated, f_a, f_w and f_{lf} will also be underestimated. The correct evaluation of the Ca uptake flux will, in principle, lead to accurate evaluations of several other Ca fluxes that are otherwise difficult to determine, such as the soil mineral weathering flux (f_w ; Eq. 1.5), or leach losses of Ca to groundwater (f_{gw}). The model values for these fluxes are computed individually for each study plot and listed in Table 5.

The average Ca weathering flux predicted by the Ca cycling model (0.019 mol m^{-2} y^{-1}; Table 5) is in good agreement with PROFILE—a steady state model developed to reconstruct

458 release rates of base cations from soil mineral weathering—yielding 0.025 mol m^{-2} y^{-1}. PROFILE
459 modeling is based on kinetic rate laws (Sverdrup, 1990) and the chemical composition of the
460 forest soil (Sverdrup and Warfvinge, 1995). The above result was obtained by modeling the first
461 50 cm of soil for each plot. Input variables included empirical mineralogy (Bélanger and
462 Holmden, submitted), specific surface area, soil water content, and soil temperature. Specific
463 surface area of the soil was calculated from an algorithm developed by Jönsson et al. (1995) using
464 measured grain size distribution, dry bulk density, and coarse fragments. Soil temperature was
465 estimated using the FORSTEM model (Yin and Arp, 1993).

466 The average Ca deposition flux predicted by the Ca cycling model (0.015 mol m^{-2} y^{-1};
467 Table 5 and Fig. 7) is within the range of wet only deposition fluxes for the Province of
468 Saskatchewan of between 0.002 and 0.030 mol m^{-2} y^{-1} (Canadian National Atmospheric
469 Chemistry Precipitation Database, 1978-1992). On the other hand, if seasonally averaged Ca
470 concentrations in precipitation from La Ronge are used from Table 2 (~0.32 ppm), then the
471 annualized atmospheric deposition flux is 0.0024 mol Ca m^{-2} y^{-1}, which is closer to the low end
472 of the provincial range represented by Cree Lake (average of 0.002 ± 0.002 mol Ca m^{-2} y^{-1}
473 measured between 1978 to 1992), one of the most pristine sites monitored in northern
474 Saskatchewan. It is important to note that the model estimation from Ca cycling is for wet and dry
475 deposition combined, whereas the provincial estimates are wet only deposition. Dry deposition
476 would need to be ~4 times higher than wet deposition to make up the difference.
477

478 5.5.2 Transient solutions

479 The impact of changing one or more Ca fluxes on soil pool $\delta^{44}Ca$ values was investigated
480 using the transient equations (1.3, 1.4) and the initial steady state Ca fluxes of plot 1.1 (Table 5).
481 Although a number of model runs were performed, two are highlighted below. The first one
482 documents changes in soil and vegetation pool $\delta^{44}Ca$ values caused by a step increase in Ca

483 uptake rate, which informs on the effects of differences in forest productivity in different regions.
484 The second one was undertaken to show the effect of changing the proposed species-specific
485 fractionation factor.

486 The impact of increasing the plant uptake flux (f_u) by 50% over the steady state value is
487 show in Fig. 8. This causes Ca concentrations to decrease in the forest floor and upper B mineral
488 soils, as expected, and δ^{44}Ca values to increase. Vegetation δ^{44}Ca increases too, because the trees
489 respond by tracking the changes in δ^{44}Ca in the soil pools. The extent to which the soil pools
490 record a heavy Ca isotope signature depends on the magnitude of the Ca uptake flux (f_u) relative
491 to the Ca input fluxes (f_a , f_{lf} , and f_w). This is shown by imposing a co-occurring increase of
492 three times the steady state flux of f_a , which is enough to reverse the increase in soil pool δ^{44}Ca
493 caused by a 50% increase in f_u (not shown). The second model run demonstrates the impact of
494 increasing Δ_{soil}^{veg} by 2.8 times and f_u by 1.4 times, which causes δ^{44}Ca values between soil and
495 vegetation pools to widen from an initial steady state separation factor of –0.7‰ ($\delta_{veg} - \delta_B$) to a
496 final separation factor of –2.3‰ (Fig. 9). These changes to the La Ronge forest Ca cycle
497 reproduces the difference in δ^{44}Ca values reported by Schmitt et al. (2003) between a beech
498 branch and soil pool measured in a forest in France.

499 Other simulations were conducted, but the results are not shown. One of these examined
500 the impact of changing the Ca uptake fractions between the forest floor and upper B mineral soil
501 on soil pool δ^{44}Ca values. Smaller soil depth gradients in δ^{44}Ca were produced in model runs
502 when most of the Ca was drawn from the forest floor ($X \approx 1$). Larger depth gradients were
503 produced when most of the Ca was drawn from the upper B horizon ($X \approx 0$). The magnitude of
504 the output flux, f_u , relative to the input fluxes f_a , f_{lf} , f_z , and f_w is another factor that
505 influences the magnitudes of the soil depth gradients. For example, if the downward flux of Ca
506 (f_z) from the forest floor is much higher than the plant uptake flux from the upper B horizon,

507 then the upper B Ca pool will mostly inherit the δ^{44}Ca value of the forest floor Ca pool, and the
508 depth gradient will be greatly diminished. Another model run (not shown) predicts that reverse
509 gradients will occur in cases where soil mineral weathering rates are high, and fine root activity is
510 concentrated in the forest floor. No reverse gradients were found among the six Boreal Shield soil
511 profiles studied in this work.
512

513 # 6. DISCUSSION

514 ## 6.1 Tracer potential of δ^{44}Ca in forested watersheds

515 The results confirm previous findings that nutrient Ca uptake by plants is a significant
516 source of isotopically fractionated Ca on the continents (Schmitt et al., 2003; Bullen et al., 2004;
517 Wiegand et al., 2005; Holmden and Bélanger, 2005; Perakis et al., 2006; Page et al., 2008; Cenki
518 Tok et al., 2009). The separation factors indicate that plant uptake favors the light isotopes of Ca,
519 which leaves the soil pools enriched in the heavy isotopes. Calcium inputs from soil mineral
520 weathering (–1.06 to –1.16‰) and atmospheric sources (–1.28‰) yield similarly low δ^{44}Ca
521 values and, therefore, cannot account for the heavy δ^{44}Ca signatures in the soil pools,
522 groundwater, or the stream. The total range of fractionation in the Boreal Shield forest, the largest
523 terrestrial biome on the planet, is ~1.6‰. Values as high as –0.45‰ characterize deeper soils and
524 shallow groundwater, and values as low as –2.2‰ characterize tree fine roots. Considering that
525 fine roots (2.0 mm) are a small component of the total mass of Ca in boreal tree species, a smaller
526 range of ~1‰ is of greater relevance in this region.
527 Once plant fractionated Ca percolates below the finely rooted zone, it is no longer
528 subjected to biological fractionation effects, and only mixing with other sources of Ca may
529 further alter its signature. This makes δ^{44}Ca a fairly unique hydrological tracer in forested
530 catchments because the heavy isotopic signature traces the source of Ca to the forest floor and
531 upper mineral soil (Schmitt et al., 2003; Holmden and Bélanger, 2006; Cenki Tok et al., 2009).

532 There are two possible exceptions to this rule. One concerns arid environments (Ewing et al,
533 2008) where soil water conditions are suitable for calcite and gypsum precipitation. The light
534 isotopes of Ca are partitioned favorably into these minerals, leaving the residual Ca in soil pore
535 fluids enriched in the heavy isotopes. The kinetic isotope fractionation governing calcite and
536 gypsum precipitation mimics the isotopic effects associated with plant uptake fractionation, and it
537 may be difficult in some environments to distinguish between them (e.g., Tipper et al., 2006;
538 Jacobson and Holmden, 2008). In acidic soils such as those of the Boreal Shield forests near La
539 Ronge, these Ca-bearing minerals do not form. It is therefore an unlikely mechanism for
540 producing heavy isotope enrichments in groundwater and surface water in Boreal Shield
541 environments.

542 The other exception concerns potential isotopic fractionation effects associated with ion
543 exchange reactions (Russell and Papanastassiou, 1978b). Because Ca filters downward through
544 the soil, its $\delta^{44}Ca$ value may be increased if ^{40}Ca is preferentially retained on ion exchange sites.
545 A lack of data on ion exchange effects prompted us to ignore the interaction between soil pore
546 waters and ion exchange pools in our model. It is assumed, for example, that the $\delta^{44}Ca$ values of
547 soil waters collected by the lysimeters genuinely reflect the $\delta^{44}Ca$ values of the Ca exchange
548 pools, and that isotope fractionation effects accompanying ion exchange reactions are small. We
549 also do not attach much importance to the modeled Ca residence times for the pools of the forest
550 floor and upper B horizons because their Ca masses are operationally defined. Nevertheless, the
551 85-year-old stands in plots 1.1, 1.2 and 2.2, which yielded relatively small Ca soil pools by the
552 $BaCl_2$ technique, have apparently attained steady state, but that the remaining plots will not reach
553 steady state in this current rotation of the forest. Recalling that the $\delta^{44}Ca$ values of the soil pools
554 are based on soil waters collected using lysimeters, it seems likely that as long as the Ca in these
555 soil waters genuinely reflects the balance of the competing input and output Ca fluxes, then the
556 most mobile fraction of the total Ca exchange pool will be close to steady state in all of the plots.

557 Although some details must await further study, the potential for $\delta^{44}Ca$ as a hydrological
558 tracer in forested catchments seems promising (Schmitt et al. 2003; Cenki Tok et al., 2009). A
559 mixing calculation shows that more than 80% of the Ca in the stream carries the heavy isotopic
560 fingerprint of the exchange pools from the surrounding forest soils. This finding is consistent with
561 conceptual models of shallow groundwater flow in first-order watersheds of the Precambrian
562 Shield. During the growing season, these watersheds are largely fed by shallow groundwater near
563 the stream and in direct contact with bedrock (Hill 2000). When it rains, the water table in the
564 saturated (riparian) zone rises and connects subsurface flow from the hillslope to the stream. The
565 lower B and C horizons are common end-members contributing to the stream during high flows
566 (Buttle and Sami 1992; O'Brien and Hendershot 1993), whereas contributions from the forest
567 floor and uppermost mineral soil occur only during floods and large snowmelt events (Bishop et
568 al. 1990; Hruska et al. 2001). For example, the hydrograph separation in O'Brien and Hendershot
569 (1993) showed that the lower mineral soil (solum) close to the stream was responsible for as
570 much as 80% of stream discharge in the summer and fall during large rain events. Moreover,
571 overland flow is normally absent in the presence of moss and well developed forest floors, and
572 direct contributions of rainfall to the stream are small due to its very small surface area. In the
573 spring, snowmelt can be a large and rapid contributor to stream discharge, but this hydrological
574 end-member is generally short-lived (Hill 2000).

575 In the studied watershed, all indications are that the hydrology is similar the above
576 conceptual model. The effect of spring snowmelt on stream discharge is no longer observable by
577 mid-May, two weeks following complete snow melt. The stream responded slightly to large rain
578 events that occurred between mid-May and mid-June, perhaps due to snow-melt saturated
579 riparian soils or remaining patches of frozen soils, both favoring rapid subsurface flow to the
580 stream. Between mid-June and September, however, changes in stream discharges during rainfall
581 were barely observable, indicating the dominance of steady groundwater feedings. Overland flow
582 was never observed, even when we were sampling during intense rain events. The relatively

583 uniform and high $\delta^{44}Ca$ value of streamwater in the La Ronge watershed, measured at the base of
584 Toposequence 1 (–0.61 ±0.05‰, 1σ) eight times in four months during the growing season,
585 confirms that direct Ca inputs to the stream from precipitation and surface runoff are minor in this
586 setting.
587
588 ## 6.2 Implications for weathering and Ca apportionment studies in trees using
589 $^{87}Sr/^{86}Sr$
590 A growing body of work using Sr isotopes has shown that a large fraction of the Ca that
591 is tightly cycled between vegetation and the forest floor is ultimately derived from atmospheric
592 sources (Miller et al., 1993; Stewart et al., 1998; Chadwick et al., 1999; Kennedy et al., 1998;
593 2002; Bullen and Bailey, 2005; Drouet et al., 2005). Recent work at La Ronge shows that Boreal
594 Shield forests are no exception to this phenomenon (Bélanger and Holmden, submitted). Simple
595 end-member mixing analysis using $^{87}Sr/^{86}Sr$ and Sr/Ca ratios applied to the six study plots from
596 both toposequences revealed that the amount of atmospherically-derived Ca in aspen, spruce, and
597 jack pine varied with landscape position. Hilltop stands sequestered more Ca from atmospheric
598 sources (85–94%) than stands at middle (47-62%) and low (37-56%) elevations (Table 5).
599 The estimates for atmospheric Ca contributions were strongly tied to the results of 1 N
600 HNO_3 leaches performed on lower B mineral soils in each plot, for the purpose of deducing soil
601 mineral weathering $^{87}Sr/^{86}Sr$ signatures (Bélanger and Holmden, submitted). However, simulating
602 natural weathering of polymineralic soils in the laboratory with acid solutions is not
603 straightforward (Blum et al., 2002, Bullen and Bailey, 2005, Drouet et al., 2005). Differences in
604 $^{87}Sr/^{86}Sr$ ratios exist among minerals, and differences in mineral weathering susceptibility yield
605 non-stoichiometric patterns of Sr release (e.g., Blum and Erel, 1997; Nezat et al., 2007).
606 Moreover, if the acid treatments are applied to lower B/C mineral soils there is the additional
607 problem of overprinting by isotopes of Sr that have filtered down from overlying soil horizons.

608 This downward flux of Sr is dominated by litterfall whose $^{87}Sr/^{86}Sr$ ratios reflect mixing between
609 atmospheric deposition and soil mineral weathering sources. Caught up on ion exchange sites, or
610 incorporated into weathered minerals, this recycled Sr must be removed before the pristine soil
611 mineral weathering $^{87}Sr/^{86}Sr$ signature can be revealed. The problem is that the $^{87}Sr/^{86}Sr$ ratio of
612 the recycled Sr component is difficult to distinguish from mineral weathering Sr component in
613 acid leached polymineralic soils. Fortunately, this is less of a problem for Ca isotopes, due to the
614 unique heavy isotope signature of plant-fractionated Ca. Calcium isotopes may be used to
615 monitor the release of recycled Sr from mineral soils, thus, fine tuning the leach protocol. An
616 examination of Fig. 6 shows that the 1 N HNO_3 leach failed to remove the heavy $\delta^{44}Ca$ signature
617 of Ca in all but two of the study plots. This means that the $^{87}Sr/^{86}Sr$ signature of soil mineral
618 weathering was likely underestimated in Bélanger and Holmden (submitted) for plots 1.2, 1.3,
619 2.1, and 2.3 and the long-term dependence of the boreal forest on atmospheric Ca contributions
620 will be slightly greater than originally calculated (Table 5).
621
622 ### 6.3 Model validation and implications for future work
623 If the atmospherically derived model Ca fluxes are correct, then the dry deposition Ca
624 flux in the La Ronge area would have to be ~4 times higher than the wet deposition flux, which
625 seems elevated. Judging from the very high 75th and 90th percentile Ca concentrations in wet
626 deposition computed from the Cree Lake database, there are rain events we did not capture in our
627 limited sampling that may be bringing in significant amounts of Ca from drier agricultural regions
628 located south of the city of Prince Albert (Fig. 1), which can carry significant amounts of Ca as
629 particulates. Indeed, a study of the impacts of a base metal smelter located at the southern edge of
630 the Precambrian Shield on the Saskatchewan-Manitoba border, East of La Ronge (McMartin et
631 al., 1999) showed that the winds are mostly coming from the northwest but also noted a
632 frequency of about 30% of winds coming from the south, southwest, or southeast. Taking this

633 into consideration lowers the divergence between modeled (wet plus dry) and measured (wet
634 only) Ca fluxes.

635 Alternatively, one or more of the model assumptions may be contributing to the relatively
636 high atmospheric Ca fluxes. A sensitivity analysis reveals two sources of uncertainty that warrant
637 further investigation. The first is the uptake flux (f_u), which scales positively with the
638 atmospheric deposition flux (f_a). If f_u is overestimated, then f_a will be overestimated, as well,
639 but the uncertainty in f_u is probably less than 20%, which is too small to significantly change the
640 large total atmospheric deposition flux calculated by the model. The second source of uncertainty
641 involves the δ^{44}Ca value of litterfall (δ_{lf}), which was assumed to be equivalent to the δ^{44}Ca value
642 of foliage in each plot. Indeed, a sensitivity analysis aimed at reducing the overall atmospheric
643 deposition flux reveals that small adjustments can be made to the value of δ_{lf} in each study plot
644 (±15%) that will result in an overall reduction of ~50% in the value of f_a. The Ca deposition flux
645 averaged overall all six study plots drops from 0.015 to ~0.008 mol m^{-2} y^{-1}. Because the modeled
646 Ca fluxes remain tuned to the Ca apportionment fractions deduced from the $^{87}Sr/^{86}Sr$ study (Table
647 5; Bélanger and Holmden, submitted), the weathering flux decreases, as well, and the proportion
648 of recycled Ca from litterfall increases from 80 to 90% of the annualized Ca inputs to the forest
649 Ca cycle. The high Ca recycling rate is consistent with Dijkstra and Smits (2002), who showed
650 that only small amounts of Ca uptake from deep soils beneath sugar maple trees were needed to
651 sustain the relatively high amounts of available Ca in the surface soil, due to tight cycling of Ca
652 through litterfall. Similar results were presented by Miller et al. (1993), upon which we based our
653 original estimate of ~80% recycling. Accordingly, our model of low Ca release from soil mineral
654 weathering, low Ca deposition rates, and tight Ca recycling, seems reasonable in the light of these
655 other studies.

We conclude that the application of the Ca cycling model to the La Ronge forest is too assumption bound to yield accurate estimates of the Ca fluxes. The main problem stems from the fact that the principal input Ca fluxes are not that widely separated from in this boreal shield setting (Table 2 and Table 4), which means that relatively small percentage changes in the input δ^{44}Ca values leads to rather large changes in the estimations of the modeled Ca fluxes. This raises the question of site selection for future studies. The δ^{44}Ca value of precipitation and soil mineral weathering should be widely separated from each other, and the litterfall return fluxes, to yield more robust estimates of Ca flux magnitudes using isotope balance modeling. Thus far, precipitation δ^{44}Ca values ranging between –0.7 and –1.7‰ have been reported (Schmitt and Stille, 2005; Cenki Tok et al., 2009), but precipitation values close to zero per mil may exist in coastal regions where Ca in rainwater is dominated by sea spray. Because most bedrock carbonates and silicates have δ^{44}Ca values of around –1‰ (DePaolo, 2004; Amini et al., 2008), field sites where precipitation values are at the extremes of the natural range may be best suited for modeling studies. A forest containing trees with a large species fractionation factor (such as beech) will help to distinguish litterfall from soil mineral weathering. In addition, a better grasp of the factors controlling litterfall δ^{44}Ca values will be important, because the litterfall flux is the largest annualized input of Ca to the forest Ca cycle.

7. CONCLUSIONS

Calcium isotope fractionation occurs in tissues formed along the transpiration stream in five boreal tree species. Fine roots yielded the lowest δ^{44}Ca values, stemwood values were intermediate, and foliage values were the highest, consistent with earlier findings (Schmitt et al., 2003; Wiegand et al., 2005; Holmden and Bélanger, 2006; Page et al., 2008; Cenki Tok et al., 2009). Plant uptake favors the light isotopes of Ca, thus leaving the residual Ca in soil pools enriched in the heavy isotopes. This implies an initial fractionation step in the tips of the fine

681 roots (Δ_{soil}^{veg}) whose magnitude appears to vary between species, but may also be subject to local
682 environmental controls (e.g., Page et al., 2008). Data on trees from this study and from the
683 literature (Schmitt et al., 2003; Bullen et al., 2004; Wiegand et al., 2005; Perakis et al., 2006;
684 Page et al., 2008; Cenki Tok et al., 2009) suggest that the degree of plant induced fractionation
685 increases in the sequence: jack pine < black spruce ≈ trembling aspen ≈ white spruce ≈ ohia <
686 beech ≈ sugar maple.

687 Experiments performed using a steady state Ca cycling model showed that the degree of
688 heavy isotope enrichment of Ca in soils is dependent on the calcium uptake rate into trees, the
689 magnitude of the fractionation factor, and the supply rates of ^{40}Ca enriched input fluxes from
690 litterfall, atmospheric deposition, and soil mineral weathering. If these latter fluxes are high
691 compared to the plant uptake flux, then the degree of ^{44}Ca enrichment in plant available soil pools
692 is diminished. All six study plots at La Ronge, however, show clear increases in soil water δ^{44}Ca
693 values with depth, ranging between 0.1 and 0.4‰. The δ^{44}Ca depth gradient appears to be the
694 most strongly developed where fine roots permeate the forest floor and upper B horizons, leveling
695 off in the deeper levels of the soil where no fine roots are found. This is evidence that soil depth
696 profiles (Perakis et al. 2008; Page et al. 2008; Cenki-Tok et al. 2009) are mostly caused by the
697 extraction of light Ca by tree fine roots rather than by ion exchange effects involving soil mineral
698 surfaces and organic ligands. It also implies that below the level of fine root activity, stable Ca
699 isotopes will behave as conservative tracers of Ca transport in soil waters, groundwaters, and
700 surface waters, so long as the ion exchange fractionation effects are small.

701 Calcium isotopes offer a new perspective on weathering and Ca apportionment studies of
702 tree nutrition using ^{87}Sr/^{86}Sr as a tracer. It is particularly challenging to apply the ^{87}Sr/^{86}Sr
703 technique to forests growing on acidic soils developed from granitic parent materials, due to the
704 large differences in mineral solubility and ^{87}Sr/^{86}Sr ratios. In addition, soils are contaminated with
705 recycled Sr released from degrading litterfall with ^{87}Sr/^{86}Sr ratios that reflect mixing of

706 isotopically distinct atmospheric and soil mineral weathering end-members. The unique heavy
707 isotope signature of plant fractionated Ca in natural soils offers a new tool for studying Ca release
708 from minerals and ion exchange sites in the laboratory by various treatments.

709 The finding that Ca isotopes are fractionated between trees and soils (Schmitt et al. 2003;
710 Wiegand et al. 2005; Holmden and Bélanger, 2006; Perakis et al. 2008; Page et al. 2008; Cenki-
711 Tok et al. 2009) brings the power of steady state and transient isotope mass balance modeling to
712 bear on a variety of questions concerning Ca cycling in forests. The soil depth gradient in $\delta^{44}Ca$ is
713 reproduced by the model, as is the range of isotopic fractionation in forested ecosystems reported
714 in the literature, thus far, by adjusting forest productivity (Ca uptake rate) and bulk fractionation
715 factor. We have shown that the Ca cycling model yields reasonable sets of relative Ca fluxes for
716 the La Ronge forest using the steady state assumption. Accuracy is compromised, however, by
717 the small range of $\delta^{44}Ca$ values found among the principle input Ca fluxes in the boreal shield
718 ecosystem. Transient solutions to the isotope mass balance equations suggest that tree ring
719 cellulose may record secular variations in $\delta^{44}Ca$ caused by natural and anthropogenic
720 disturbances to the forest Ca cycle.
721

722 ## ACKNOWLEDGMENTS

723 Tim Prokopiuk is thanked for assistance in the laboratory. We also thank A. Taylor, S.
724 Friessen, M. Emigh, J. Jackson and N. Roberston for their hard work in the field and laboratory.
725 Dimiti Papanastassiou is thanked for advice and assistance concerning the mass spectrometry of
726 calcium, and for hosting C.H. during a sabbatical visit to Caltech in 2003. C.H. also thanks
727 Johannes Schwieters for communications that have guided certain tests, and clarified some of the
728 findings reported in Appendix A. The field study and sampling was made possible *via* the
729 financial support to N. Bélanger from the Natural Science and Engineering Council of Canada
730 (Discovery grant). The authors thank Frank Podosek (editor) and associate editors Alan Brandon

and Martin Novak for their comments and handling of the review process. We thank two anonymous reviewers whose careful reading of the manuscript helped to improve the presentation.

APPENDIX A. FACTORS INFLUENCING HIGH PRECISION MEASUREMENTS OF Ca ISOTOPES

It is widely acknowledged that Ca isotopes are difficult to measure (e.g., DePaolo, 2004), but for reasons that are not entirely clear. Over the past ten years, the range of precision reported in the literature has varied widely. DePaolo et al. (2004) reported good internal precision (~0.05‰) for Ca isotope measurements using a multi-collector technique on a VG 354 instrument, but poor sample reproducibility (external precision, ±0.5‰ 2σ). This was attributed to subtle ion beam focusing differences between samples. Fletcher et al. (1997) also reported difficulties with static multi-collection measurements on a VG 354 instrument and believed that ion optical effects were to blame. Heuser et al. (2002) published a multi-collection routine for Ca isotope measurements on a Finnigan-MAT 262 instrument, but were unable to show improved external precision over single collector peak hopping measurements performed on the same instrument (±0.25‰, 1σ). Because $^{44}Ca/^{40}Ca$ variability in the sub ~1‰ range is common, any improvement in precision and accuracy that may be related to mass spectrometer performance, choice of double spike, sample loading, or the limitations of the instrumental mass fractionation law, would be a welcome advance. For this reason, we briefly describe our experience measuring Ca isotopes in the Saskatchewan Isotope Laboratory (SIL) over the past four years, including the adopted best practices for achieving reproducibility of ±0.07‰ (2σ) on the $^{44}Ca/^{40}Ca$ ratio.

The Ca isotope measurements were performed on a Thermo-Finnigan Triton instrument using a ^{43}Ca-^{42}Ca double spike to correct for instrumental mass fractionation. The rationale for using ^{43}Ca-^{42}Ca, as opposed to more common double-spikes with ^{48}Ca, is discussed in Holmden

(2005) and Gopalan et al. (2006). The initial motivation was to restrict the mass range of the four isotopes needed for a mass bias corrected measurement of $^{44}Ca/^{40}Ca$ to 5% by making the measurements in two scans or 'hops' of the magnetic field. Since then, a third hop was added so that all isotope ratios could be constructed from ion beams that were collected symmetrically with respect to the ion optical axis of the instrument. It was reasoned that this configuration would allow ion beams to strike their respective collectors in roughly the same place, at roughly similar angles to the image plane of the detector array, thus coming as closely as possible to negating potential differences in cup efficiencies that might result from non-linear changes in ion optical properties across the collector array (Fletcher et al., 1997). The collector configuration used is shown in Fig. 10.

Moreover, performing the measurements in a sequence of hops enables the signal integration times to be optimized for differences in ion beam intensities of the collected masses (particularly severe for the Ca mass spectrum, which consists of one abundant isotope and five minor isotopes). This flexibility allows scans of the smaller ion beams to be integrated for longer periods of time, thus improving the ion counting statistics, while at the same time limiting the collection of the largest ion beam (^{40}Ca) to a short integration time in order to limit any potential degradation in the performance of the collector (Fig 10). In addition, potential ^{40}K interference on ^{40}Ca can be monitored using the ^{41}K abundance measured in the axial collector of the first scan.

With ion optical effects minimized a suspected drift in instrument performance could be better evaluated. It had been noticed over the course of development that there were significant periods of a few weeks duration when the reproducibility of Ca isotope standards was significantly better than at other times. We attributed this drift to changes in collector efficiencies. In an attempt to solve this problem we first installed new graphite collectors in October 2006. After changing the graphite collectors, the first measurements of the CaF_2 and Pacific seawater standards came out 0.19‰ lower in $\delta^{44}Ca$ value, which seemed to confirm cup damage, but the standards changed again within a few weeks of installing the new cups (Fig. 11).

Figure 11 was constructed using data from 43 measurement sessions conducted over the past, approximately, three years. Each session included measurements of the SIL CaF_2 'isotopic normal' as well as natural seawater. Some sessions also included measurements of SRM 915a. To account for the instrumental drift, the spike composition was adjusted for each session using an exponential mass fractionation law so as to yield the $^{40}Ca/^{44}Ca$ ratio of the SIL CaF_2 standard of 47.153 and the seawater ratio of 47.092. In essence, each measurement session reflects a new calibration of the double spike based on spiked analyses of these internal standards. Figure 11 records the long term pattern of adjustments made to the $^{43}Ca–^{42}Ca$ ratio of the double-spike required to adjust for the instrumental drift. This is shown on the y-axis, on the right hand side of the diagram. The y-axis on the left hand side of the diagram shows the nominal per mil deviations in $\delta^{44}Ca$ values that will result from these adjustments in spike composition. In other words, if the drift correction is not applied, the $\delta^{44}Ca$ measurements of samples will drift in time by the amount shown on the left hand y-axis. Accordingly, if the drift is not carefully monitored and corrected for with standards, the long term reproducibility of $\delta^{44}Ca$ is quite poor (±0.23‰, 2σ).

The best data is obtained for short sessions of about two weeks with 15–30 measurements completed, including standards. In the last 24 sessions, 41 $^{44}Ca/^{40}Ca$ measurements of CaF_2 and 49 measurements of seawater were measured (excluding measurements whose δ values were sufficiently errant to warrant termination of the session). The average difference between the seawater and the CaF_2 standards is –1.29 ±0.03‰ (2σ). The relatively low uncertainty benefits from taking the difference of averages of the two standards from each session, which minimizes the impact of outliers. A better sense of the reproducibility for a single measurement is estimated by taking the average standard deviation of 90 measurements of CaF_2 and seawater over the last 24 sessions, which combined yields ±0.07‰ (2σ). The $\delta^{44}Ca$ value of 915a measured over the same period is –1.86 ±0.05‰ (2σ, n=13)

A close examination of Fig. 11 shows that the shift that occurred when the collectors were changed is not the largest shift observed over the recorded period. Therefore, swapping out the collectors does not solve the drift problem permanently. In addition, the shifts occur in both directions from the mean. Visual inspection of the graphite collectors removed from our machine showed that the formerly matte black collectors showed a luster over large areas (Fig. 12). The luster (which appears lighter or white in the photographs) is more prominent on one side of the collector than the other. Imaging of the original black and high luster areas of the collector using an electron microscope picked up no differences in elemental composition between them using an energy dispersive spectrometer, but differences in surface texture are visible (Fig. 13). The surfaces showing luster (white) are smoother than the original matte black areas of the collectors. We believe that the smoothing is caused by Ca ion beams hitting the sides of their respective collectors.

The angles of the collectors are factory set in order to optimize the collection of Nd isotopes, such that each ion beam in the Nd mass spectrum squarely impacts the back of its dedicated collector. Considering just four isotopes of Nd, the collector angles are optimized for a mass range of ~2.7%. The same collectors used to measure four adjacent isotopes of Ca must accommodate a mass range of 9.5%. Consequently, the Ca ion beams hit the sides of their collectors, which may cause carbon to sputter from the low angles of interception, thus smoothing the surface of the collector over time. If the smoothing causes changes in collector efficiencies, then a physical explanation for the instrumental drift in Ca isotope measurements may have been found. But the smoothing phenomenon alone does not explain the fact that the drift is reversible (Fig. 11), unless the surface chemistry of the collector is also affected. We have noticed that the stability of the collector efficiencies is improved by running other elements into the collectors. The reason for this is unclear, but given the evidence for cup ablation in Fig. (12), and the interception of the Ca ion beams along the sides of the collectors, running other ions into the collectors might help to remove monolayers of calcium that may coat the surface of the collector

over long analysis sessions, or shorter sessions with large ion beam intensities, thus changing the surface insulating properties of the collector surface.

Although speculative, the hypothesis has merit because it helps to explain the improved reproducibility in $\delta^{44}Ca$ that we obtain in the Saskatchewan Isotope Laboratory using a ^{43}Ca–^{42}Ca double spike coupled with dynamic collection, as compared to most other laboratories using ^{48}Ca–^{42}Ca or ^{48}Ca–^{43}Ca double spikes. Specifically, the ^{43}Ca–^{42}Ca double spike allows for a reduction in the integration time for the large ^{40}Ca ion beam (presumably reducing the rate of build up of Ca ions on the collector surface), and a reduction in the angles of interception for all Ca ion beams with their respective collectors by restricting the mass range of measured Ca isotopes (i.e., increasing the depth of penetration of the ions into the collector). In addition, collecting the ion beams symmetrically with respect to the axial collector may reduce effects resulting from to non-linear changes in ion optical properties across the image plane (Fletcher et al., 1997).

REFERENCES

Amini M., Eisenhauer A., Böhm F., Holmden C., Kreissig K., Hauff F., Jochum K. P. 2008. Calcium isotopes in MPI-DING Reference Glasses, USGS rock powders and various rocks: evidence for Ca isotope fractionation in terrestrial silicates. Geostandards Newsletter 33, 231–247.

Bélanger N. and Holmden C. Apportionment study of Ca nutrition in a Boreal Shield forest of Saskatchewan (Canada) using $^{87}Sr/^{86}Sr$ as a tracer, submitted to *Ecosystems*.

Bishop, K. H., Grip, H. and O'Neill, A. (1990) The origins of acid runoff in a hillslope during storm events, J. Hydrol. 116, 35–61.

Blum J. D. and Erel Y. (1997) Rb-Sr isotope systematics of a granitic soil chronosequence: The

857 importance of biotite weathering. *Geochim. Cosmochim. Acta* 61, 3193–3204.

858 Blum J. D., Klaue A., Nezat C. A., Driscoll C. T., Johnson C. E., Siccama T. G., Eagar C., Fahey
859 T. J. and Likens G. E. (2002) Mycorrhizal weathering of apatite as an important Ca source
860 in base-poor forest ecosystems. *Nature* 417, 729–731.

861 Bullen T. D., Fitzpatrck J. A., White A. F., Schulz M. S. and Vivit D. V. (2004) Calcium stable
862 isotope evidence for three soil calcium pools at a granitoid chronosequence. In *Water-Rock*
863 *Interaction, Proceedings of the Eleventh International Symposium on Water-Rock*
864 *Interaction*, vol. 1 (eds. R. B. Wanty and R. R. Seal II). Taylor and Francis, London, pp.
865 813–817.

866 Bullen T. D. and Bailey S. W. (2005) Identifying calcium sources at an acid deposition-impacted
867 spruce forest: a strontium isotope, alkaline earth element multi-tracer approach.
868 *Biogeochem.* 74, 63–99.

869 Buttle, J.M., Sami, K. (1992) Testing the groundwater ridging hypothesis of streamflow
870 generation during snowmelt in a forested catchment. J. Hydrol. 135, 53–72.

871 Canadian National Atmospheric Chemistry Precipitation Database (1978-1992). Environment
872 Canada, Meteological Service of Canada, Toronto, ON.

873 Cenki Tok B., Chabaux F., Lemarchand D., Schmitt A-D., Pierret M-C., Viville D., Bagard M-L.,
874 Stille P. 2009. The impact of water-rock interaction and vegetation on calcium isotope
875 fractionation in soil-and stream waters of a small, forested catchment (the Strengbach case).
876 Geochimica et Cosmochimica Acta 73, 2215–2228.

877 Chadwick O. A., Derry L. A., Vitousek P. M., Huebert B. J. and Hedin L. O. (1999) Changing
878 sources of nutrients during four million years of ecosystem development. *Nature* 397, 491–
879 497.

880 DePaolo D. J. (2004) Calcium isotope variations produced by biological, kinetic, radiogenic, and
881 nucleosynthetic processes. In *Geochemistry of Non-traditional Stable Isotopes* (eds. C. M.
882 Johnson, B. L. Beard and F. Albarede). Reviews in Mineralogy, Mineralogical Society of
883 America, Washington DC, pp. 255–288.
884 Dijkstra F. A. and Smits M. M. (2002) Tree species effects on calcium cycling: The role of
885 calcium uptake in deep soils. *Ecosystems* 5, 385–398.
886 Drouet Th, Herbauts J., Gruber W. and Demaiffe D. (2005) Strontium isotope composition as a
887 tracer of calcium sources in two forest ecosystems in Belgium. *Geoderma* 126, 203–23.
888 Eugster O., Tera F. and Wasserburg G. J. (1969) Isotopic analysis of barium in meteorites and in
889 terrestrial samples. *J. Geophys. Res.* 74, 3897–3908.
890 Ewing S. A., Yang W., DePaolo D. J., Michalski G., Kendall C., Stewart B. W., Thiemens M.
891 and Amundson R. (2008) Non-biological fractionation of stable Ca isotopes in the Atacama
892 Desert, Chile. *Geochim. Cosmochim. Acta* 72, 1096–1110.
893 Fantle M.S. and DePaolo D.J. (2005) Variations in the marine Ca cycle over the past 20 million
894 years. *Earth Planet. Sci. Lett.* 237, 102–117.
895 Fantle M. S. and DePaolo D. J. (2007) Ca isotopes in carbonate sediment and pore fluid from
896 ODP Site 807A: The Ca^{2+}(aq)-calcite equilibrium fractionation factor and calcite
897 recrystallization in Pleistocene sediments. *Geochim. Cosmochim. Acta* 71, 2524–2546.
898 Fantle M. S. and Bullen T. D. (2009) Essentials of iron, chromium and calcium isotope analysis
899 of natural materials by thermal ionization mass spectrometry. *Chem. Geol.* 258, 50–64.
900 Farkas J., Bohm F., Wallmann K., Blenkinsop J., Eisenhauer A., Geldren R. V., Munnecke A.,
901 Voigt S. and Veizer J. (2007) Calcium isotope record of Phanerozoic oceans: Implications
902 for chemical evolution of seawater and its causative mechanisms. *Geochim. Cosmochim.*
903 *Acta* 71, 5117–134.

904 Fletcher I. R., Maggi A. L., Rosman K. J. R. and McNaughton N. J. (1997) Isotopic abundance
905 measurements of K using a wide-dispersion multi-collector mass spectrometer and low-
906 fractionation ionisation techniques. *Int. J. Mass Spectrom. Ion Proc.* 163, 1–17.

907 Gopalan K., Macdougall D. and Macissaac C. (2006) Evaluation of a Ca-42-Ca-43 double spike
908 for high precision Ca isotope analysis. *International Journal of Mass Spectrometry* 248, 9-
909 16.

910 Gussone N., Eisenhauer A., Heuser A., Dietzel M., Bock B., Bohm F., Spero H. J., Lea D. W.,
911 Bijma J. and Nagler T. F. (2003) Model for kinetic effects on calcium isotope fractionation
912 in inorganic aragonite and cultured planktonic foraminifera. *Geochim. Cosmochim. Acta*
913 67, 1375–1382.

914 Gussone N., Bohm F., Eisenhauer A., Dietzel M., Heuser A., Teichert B. M. A., Reitner J.,
915 Worheide G. and Dullo W-C. (2005) Calcium isotope fractionation in calcite and aragonite.
916 *Geochim. Cosmochim. Acta* 69, 4485–4494.

917 Hart S. R. and Zindler A. (1989) Isotope fractionation laws – a test using calcium. *Int. J. Mass*
918 *Spectrom. Ion Proc.* 89, 287–301.

919 Heuser A., Eisenhauer A., Gussone N., Bock B., Hansen B. T. and Nagler Th. F. (2002)
920 Measurement of calcium isotopes (δ^{44}Ca) using a multicollector TIMS technique. *Int. J.*
921 *Mass Spectrom.* 220, 385–397.

922 Hill, A.R. (2000) Stream chemistry and riparian zones In: Streams and Ground Waters, J.B. Jones
923 and P.J. Mulholland (Eds). Academic Press, San Diego, CA. pp. 83–110.

924 Hippler D., Schmitt A.D., Gussone N., Heuser A., Stille P., Eisenhauer A. and Nägler T.F. (2003)
925 Calcium isotopic composition of various reference materials and seawater. Geostandards
926 Newsletter: The Journal of Geostandards and Geoanalysis 27, 13–19.

927 Holmden C. and Bélanger N. (2006) Calcium isotope fractionation in a boreal forest ecosystem.
928 *Geochim. Cosmochim. Acta* 70, (18) A261–A261 suppl. S, AUG–SEP.

929 Holmden C. (2005) Measurement of $\delta^{44}Ca$ using a ^{43}Ca–^{42}Ca double-spike TIMS technique. In
930 *Summary of Investigations 2005*, Volume 1. Saskatchewan Geological Survey,
931 Saskatchewan Industry and Resources, Misc. Rep. 2005-1,CD-ROM, Paper A-4, 7p.
932 Hruska, J., Laudon, H., Johnson, C.E., Köhler, S., and Bishop, K. (2001) Acid/base character of
933 organic acids in a boreal stream during snowmelt. Water Resources Research 37, 1043–
934 1056.
935 Jacobson A. D. and Holmden C. (2008) $\delta^{44}Ca$ evolution in a carbonate aquifer and its bearing on
936 the equilibrium isotope fractionation factor for calcite. *Earth Planet. Sci. Lett.* 270, 349–
937 353.
938 Jönsson C., Warfvinge P. and Sverdrup H. (1995) Application of the SAFE model to the Solling
939 spruce site. *Ecol. Model.* 83, 85–96.
940 Kalyn A. L. and Van Rees K. C. J. (2006) Contribution of fine roots to ecosystem biomass and
941 net primary production in blackspruce, aspen, and jack pine forests in Saskatchewan.
942 *Agricult. Forest Meteor.* 240, 236–243.
943 Kennedy M. J., Chadwick O. A., Vitousek P. M., Derry L. A. and Hendricks D. M. (1998)
944 Changing sources of base cations during ecosystem development, Hawaiian Islands.
945 *Geology* 26, 1015–1018.
946 Kennedy M. J., Hedin L. O. and Derry L. A. (2002) Decoupling of unpolluted temperate forest
947 from rock nutrient sources revealed by natural $^{87}Sr/^{86}Sr$ and ^{84}Sr tracer addition. *Proc. Natl.*
948 *Acad. Sc.* 99, 9639–9644.
949 Lemarchand D., Wasserburg G. J. and Papanastassiou D. A. (2004) Rate-controlled calcium
950 isotope fractionation in synthetic calcite. *Geochim. Cosmochim. Acta.* 68, 4665–4678.
951 Lambert M. C, Ung C. H. and Raulier F. (2005) Canadian national tree aboveground biomass
952 equations. *Can. J. For. Res.* 35, 1996–2018.
953 MacDonald J. D., Bélanger N., Sauvé S., Courchesne F. and Hendershot W. H. (2007) Collection

954 and characterization of soil solutions. In *Soil Sampling and Methods of Analysis* (eds. M.
955 R. Carter and E. G. Gregorich), 2nd edition. CRC Press, Boca Raton.
956 McMartin I, Henderson P. J. and Nielsen E. (1999) Impact of a base metal smelter on the
957 geochemistry of soils of the Flin Flon region, Manitoba and Saskatchewan. *Can. J. Earth*
958 *Sci.* 36,141–160.
959 Miller H. G. (1995) The influence of stand development on nutrient demand, growth and
960 allocation. *Plant Soil* 168, 225–232
961 Miller E. K., Blum J. D. and Friedland A. J. (1993) Determination of soil exchangeable-cation
962 loss and weathering rates using Sr isotopes. *Nature* 362, 438–441.
963 Nezat C. A., Blum J. D., Yanai R. D. and Hamburg, S. P. (2007) A sequential extraction to
964 determine the distribution of apatite in granitoid soil mineral pools with application to
965 weathering at the Hubbard Brook Experimental Forest, NH, USA. *Appl. Geochem.* 22,
966 2406–2421.
967 Obrien C. and Hendershot W. H. (1993) Separating streamflow into groundwater, solum and
968 upwelling flow and its implications for hydrochemical modeling. *J. Hydrol.* 146, 1–12.
969 Page B. D., Bullen T. D. and Mitchell M. J. (2008) Influences of calcium availability and tree
970 species on Ca isotope fractionation in soil and vegetation. *Biogeochem.* 88, 1–13.
971 Perakis S. S., Maguire D. A., Bullen T. D., Cromack K., Waring R. H. and Boyle J. R. (2006)
972 Coupled nitrogen and calcium cycles in forests of the Oregon Coast Range. *Ecosystems* 9,
973 63–74.
974 Russell W. A. and Papanastassiou D. A. (1978a) Ca isotope fractionation on the Earth and other
975 solar system materials. *Geochim. Cosmochim. Acta* 42, 1075–1090.
976 Russell W. A. and Papanastassiou D. A. (1978b) Ca isotope fractionation in ion-exchange
977 chromatography. *Analyt. Chem.* 50, 1151–1154.
978 Saskatchewan Environment (2006) http://gisweb1.serm.gov.sk.ca/publicweb/Map_Gallery/Fire
979 /pdf/Historical_1945_2006.pdf

980 Schmit A-D., Chabaux F. and Stille P. (2003) The calcium riverine and hydrothermal isotopic
981 fluxes and the oceanic calcium mass balance. *Earth Planet. Sci. Lett.*, 213, 503–518.
982 Schmitt A-D. and Stille P. (2005) The source of calcium in wet atmospheric deposits: Ca-Sr
983 isotope evidence. *Geochim. Cosmochim. Acta* 69, 3463–3468.
984 Skulan J. L., De Paolo D. J. and Owens T. L. (1997) Biological control of calcium isotopic
985 abundances in the global calcium cycle. *Geochim. Cosmochim. Acta* 61, 2505–2510.
986 Sime N. G., De La Rocha C. L. and Galy A. (2005) Negligible temperature dependence of
987 calcium isotope fractionation in 12 species of planktonic foraminifera. *Earth Planet. Sci.*
988 *Lett.* 232, 51–66.
989 Steuber T. and Buhl D. (2006) Calcium-isotope fractionation in selected modern and ancient
990 marine carbonates. *Geochim. Cosmochim. Acta* 70, 5507–5521.
991 Stewart B. W., Capo R. C. and Chadwick O. A. (1998) Quantitative strontium isotope models for
992 weathering, pedogenesis and biogeochemical cycling. *Geoderma* 82, 173–195.
993 Sverdrup H. U. (1990) *The kinetics of base cation release due to chemical weathering*. Lund
994 University Press, Lund, Sweden, 246 p.
995 Sverdrup H. and Warfvinge P. (1995) Critical loads of acidity for Swedish forest ecosystems.
996 *Ecol. Bull.* 44, 75–89.
997 Tipper E.T., Galy A. and Bickle M.J. (2006) Riverine evidence for a fractionated reservoir of Ca
998 and Mg on the continents: Implications for the oceanic Ca cycle. *Earth Planet. Sci. Lett.*
999 247, 267–279.
1000 Upadhyay D., Scherer E. E. and Mezger K (2008) Fractionation and mixing of Nd isotopes
1001 during thermal ionization mass spectrometry: implications for high precision $^{142}Nd/^{144}Nd$
1002 analyses. *J. Analyt. Atom. Spectrom.* 23, 561–568.
1003 Wiegand B. A, Chadwick O. A., Vitousek P. M. and Wooden J. L. (2005) Ca cycling and isotopic
1004 fluxes in forested ecosystems in Hawaii. *Geophys. Res. Lett.* 32, L11404. Doi:
1005 10.1029/2005GLO22746.

1006 Yin X. and Arp P. A. (1993) Predicting forest soil temperatures from monthly air temperature and
1007 precipitation records. *Can. J. For. Res.* 23, 2521–2536.
1008 Zhu P. and MacDougall J. D. (1998) Calcium isotopes in the marine environment and the oceanic
1009 calcium cycle. *Geochim. Cosmochim. Acta* 62, 1691–1698.

1010

1011 Figure Captions

1012 Fig. 1. Map of Saskatchewan, Canada, showing the location of the study area in relation to
1013 ecozones and population centers. Sites identified with the target symbol are locations where Ca
1014 has been measured in wet deposition by Environment Canada (see Fig. 7).

1015

1016 Fig. 2. Schematic illustration of the topography of Toposequence 1 in the Boreal Shield study
1017 site near La Ronge, Saskatchewan, showing the first order stream, study plot locations, soil types,
1018 and major tree species. Shown are δ^{44}Ca values for vegetation, soil pools, groundwater, granite
1019 bedrock, seasonally averaged precipitation, and the average value for eight measurements of the
1020 stream taken from the 2005 field season. Two δ^{44}Ca values for each tree are shown: the upper
1021 value represents foliage; the lower value represents stemwood. This toposequence supports a
1022 mixedwood forest.

1023

1024 Fig. 3. Schematic illustration of the topography of Toposequence 2, located 40 m upstream from
1025 Toposequence 1. Shown are δ^{44}Ca values for vegetation and soil pools (see Fig. 2 for additional
1026 information). This toposequence supports a black spruce/feathermoss forest.

1027

1028 Fig. 4. Two-box model of the forest Ca cycle highlighting the impact of atmospheric deposition,
1029 soil mineral weathering, and plant uptake on the isotope balance of Ca in the plant available Ca

pools of the forest floor and upper B horizon. Soil depth thickness of each Ca pool is also shown. Model parameters and system components are defined in Table 1.

Fig. 5. Relationship between $\delta^{44}Ca$ values in stemwood and foliage samples collected from the six study plots. The y-intercept gives a sense of the magnitude of the Ca isotope fractionation between foliage and stemwood.

Fig. 6. Plot of $^{87}Sr/^{86}Sr$ *vs.* $\delta^{44}Ca$ for extracts and acid leaches of lower B/C mineral soils from each study plot. The acid leaches were performed in order to determine the Sr and Ca isotope compositions of the soil mineral weathering end-member. The paths joining sample points reflect (from right to left) the sequential treatments applied to each soil sample in the following order: 0.1 N $BaCl_2$–1 N HNO_3–15 N HNO_3. The $^{87}Sr/^{86}Sr$ ratios increase and $\delta^{44}Ca$ values decrease with increasing strength of treatment. The $\delta^{44}Ca$ trends appear to reach plateau values of either –1.06 or –1.16‰ (gray bands) that additional leaching is unlikely to change. By contrast, $^{87}Sr/^{86}Sr$ ratios steadily increase with each successively more aggressive treatment, indicating fractional increases in the Sr contributions from biotite and possibly K-feldspar.

Fig. 7. Measurements of Ca in wet deposition from three sites in Saskatchewan (Canadian National Atmospheric Chemistry Precipitation Database (1978-1992)). The dashed line indicates the seasonally averaged wet deposition flux of Ca at the La Ronge study site (0.0024 mol Ca m^{-2} y^{-1}) measured from data collected as part of this study.

Fig. 8. The initial steady state $\delta^{44}Ca$ values for plot 1.1 are shown to the left of the diagram for the forest floor and upper B soil pools. The $\delta^{44}Ca$ value of the vegetation is also shown. An increase of 50% in the Ca uptake flux causes the $\delta^{44}Ca$ values of both soil vegetation pools to

1055 increase as the system adjusts to the new steady state condition. The time needed to reach steady
1056 state is a function of the mass of Ca in the soil pools.
1057
1058 Fig. 9. The initial steady state $\delta^{44}Ca$ values for plot 1.1 are shown to the left of the diagram for
1059 the forest floor and upper B soil pools. The $\delta^{44}Ca$ value of the vegetation is also shown. The
1060 initial steady state was perturbed in two ways: forest productivity (the Ca uptake rate) was
1061 increased by 1.4 times, and the species specific Ca isotope fractionation factor (Δ_{soil}^{veg}) was
1062 increased 2.8 times. The new steady state condition is characterized by lower $\delta^{44}Ca$ values in
1063 vegetation and a more dramatic $\delta^{44}Ca$ gradient with soil depth. The shift in the forest floor Ca
1064 pool towards lower $\delta^{44}Ca$ values reflects the interplay between increased Ca uptake rate and
1065 decreased $\delta^{44}Ca$ of litterfall caused by the increase in the fractionation factor.
1066
1067 Fig. 10. Faraday collector configuration used for Ca isotope measurements. The duty cycle
1068 consists of three mass scans. Isotope masses are collected symmetrically with respect to the axial
1069 collector. Signal integration times are given in parentheses in units of seconds (s).
1070
1071 Fig. 11. Plot showing the range in instrumental drift of the Triton instrument over a three-year
1072 period. The magnitude of the drift is quantified by monitoring adjustments made to the ^{43}Ca–^{42}Ca
1073 ratio of the double spike (using an exponential law) required to negate the effect of the drift on
1074 the reproducibility of the 'absolute' $^{44}Ca/^{40}Ca$ ratios of the CaF_2 and seawater standards. If the
1075 drift is not corrected for, then the long-term reproducibility is poor (on the order of ±0.23‰
1076 (2σ)). On the other hand, the reproducibility is much improved (±0.065‰, 2σ) if a drift
1077 correction is applied by closely monitoring the standards. Instrumental drift, however, is not the
1078 only factor that influences the external precision of the measurements. Reproducible loading,
1079 focusing, and mass fractionation during the run are also important. When these additional factors

1080 are tightly controlled, the reproducibility ultimately rests on the analyst's ability to recognize and
1081 correct for effects of instrumental drift. To validate our approach, 13 measurements of SRM 915a
1082 were performed at least once in 13 different sessions over the past two years, yielding –1.86
1083 ±0.05‰ (2σ). Although the instrumental drift was ~0.3‰ over this period, the measurements of
1084 915a fall within a total range of 0.1‰, at the 95% confidence level. A similar drift correction
1085 could be made by normalization to a sequence of standards run at the same time as a sequence of
1086 samples.
1087
1088 Fig. 12. Original (factory installed in 2002) L2 Faraday collector graphite inserts from the SIL
1089 Triton instrument used to collect ^{40}Ca according to the collector configuration in Holmden
1090 (2005). The graphite inserts for eight moveable collectors were replaced October 6, 2006. Most of
1091 the collectors showed a luster over large areas of their surfaces (the lighter or whiter areas in the
1092 photographs). New collectors show a matte black appearance in reflected light.
1093
1094 Fig. 13. Electron microscopy image of the L2 collector. A. The black areas of the collector seen
1095 in Fig. 12 have rough surfaces; the white areas have smooth surfaces. The white areas are where
1096 the ion beams hit the collector (Magnification is 250 times). B. Close-up image of the white area
1097 in 13A, showing altered smooth surface of collector (2500 times). C. Close-up image of the black
1098 area in 13A showing original rough surface of collector (2500 times). D. Close-up image of the
1099 transitional area between smooth and rough textured surfaces found along the inner edge of the
1100 collector.
1101

Table 1. Definitions for model variables and system components

Variables	Description	Units
M_i	moles of Ca in component i per unit area	mol m^{-2}
f_i	flux density of Ca for component i	mol m^{-2} y^{-1}
δ_i	δ^{44}Ca value of component i	‰
Δ_{i1}^{i2}	fractionation factor between components 1 and 2	‰
X	fraction of Ca taken up by fine roots in forest floor compared to upper B horizon	
Components (*i*)		
veg	trees	
FF	forest floor	
B	upper B horizon permeated by fine roots	
soil	combined forest floor and upper B soil pools	
stem	stemwood	
foliage	foliage	
B/C	lower B horizon (BC) below finely rooted soil	
a	atmospheric deposition	
w	weathering	
lf	litterfall	
u	plant uptake	
z	leach loss from forest floor	
gw	leach loss to groundwater	

Table 2. Ca and Sr isotopic and elemental data for the La Ronge watershed

Sample Description	$\delta^{44}Ca$ (‰ seawater)	2 s.e.	Ca (ppm)	$^{87}Sr/^{86}Sr$[1]
Precipitation				
Summer —open field (above canopy)				
BP3 July 6/05	-1.31	0.04	0.496	——
BP3 July 14/05	——	——	0.472	——
BP3 July 30/05	-1.31	0.05	0.168	——
Average	-1.31		0.379	
Snow pack				
Nemeiben Lake 1	-1.21	0.05	0.135	——
Nemeiben Lake 2	-1.20	0.05	0.212	——
Lac La Ronge 1	-1.41	0.04	0.178	——
Lac La Ronge 2	-1.25	0.04	0.195	——
Average	-1.22		0.180	
Average Precipiation				
(30%) and rain (70%)	-1.28		0.319	
Toposequence 1				
Plot 1.1				
Foliage				
Jack Pine	-0.64	0.06	6285	——
Trembling Aspen	-1.30	0.05	12703	——
Black Spruce (young)	-1.07	0.04	6254	——
Black Spruce (old)	-1.20	0.04	10071	——
Stemwood				
Jack Pine	-1.14	0.06	1268	——
Trembling Aspen	-1.79	0.04	3274	——
Black Spruce (old)	-1.58	0.05	1761	——
Roots				
Jack Pine 2.0 mm	-1.57	0.05	3053	——
Trembling Aspen 2.0 mm	-2.18	0.10	4166	——
Soil pools (lysimeters)				
Forest floor horizon (~10 cm depth)	-1.02	0.04	6.40	——
Upper B horizon (~35 cm depth)	-0.79	0.05	——	——
Extracts and acid leaches (B/C horizon, 50–65 cm depth)				
$BaCl_2$	-0.80	0.03	41.1	0.7143
1N HNO3	-1.14	0.04	314	0.7155
15N HNO3	-1.05	0.05	629	0.7394
Residue	——	——	——	0.7074
Plot 1.2				
Foliage				
jack Pine	-0.65	0.07	6794	——
trembling Aspen	-0.96	0.04	15443	——
black Spruce (young)	-1.31	0.06	7742	——
black Spruce (old)	-1.24	0.05	3748	——
Stemwood				
jack Pine	-1.19	0.05	1001	——
trembling Aspen	-1.44	0.06	1915	——
black Spruce (old)	-1.68	0.05	1894	——
Roots				
trembling Aspen 0.5 mm	-1.26	0.04	2593	——
trembling Aspen 2.0 mm	-2.03	0.03	4769	——
black Spruce 2.0 mm	-2.11	0.04		
Soil pools (lysimeters)				
Forest floor horizon (~10 cm depth)	-1.05	0.05	16.6	——
Upper B horizon (~35 cm depth)	-0.69	0.06	6.23	——
Extracts and acid leaches (B/C horizon, 50–65 cm depth)				
$BaCl_2$	-0.56	0.04	117	0.7112
1N HNO3	-0.95	0.04	604	0.7327
15N HNO3	-1.06	0.04	829	0.7497
residue	——	——	——	0.7070
Plot 1.3				
Foliage				
trembling Aspen	-0.89	0.04	13612	——
black Spruce (young)	-1.34	0.05	6050	——
black Spruce (old)	-1.31	0.05	11030	——
white Spruce	-1.32	0.05	12911	——
balsam Poplar	-0.90	0.04	13684	——
Stemwood				
trembling Aspen	-1.40	0.04	2120	——
black Spruce (old)	-1.60	0.06	1658.25	——
white Spruce	-1.64	0.04	995.00	——
balsam Poplar	-1.65	0.04	4987	——
Soil pools (lysimeters)				
Forest floor horizon (~10 cm depth)	-0.85	0.04	7.46	——
Ah (~20 cm depth)	-0.55	0.06	7.58	——
Upper B horizon (~35 cm depth)	-0.45	0.03	10.22	——
Groundwater				
1.4m	-0.57	0.10	13.17	——
1.8 m	-0.60	0.06	27.53	——
Extracts and acid leaches (B/C horizon, 50–65 cm depth)				
$BaCl_2$	-0.68	0.03	2393	0.7354
1N HNO3	-0.81	0.03	1233	0.7471
15N HNO3	-1.14	0.04	1455	0.7774
residue	——	——	——	0.7240

1.See Bélanger and Holmden (submitted) for complete $^{87}Sr/^{86}Sr$ dataset

Table 2. (continued)

Sample Description	$\delta^{44}Ca$ (‰ seawater)	2 s.e.	Ca (ppm)	$^{87}Sr/^{86}Sr$[1]
Toposequence 2				
Plot 2.1				
Foliage				
Black spruce - a	-1.27	0.04	16756	——
Black spruce - b	-1.04	0.04	9471	——
Stemwood				
Black spruce - b	-1.26	0.04	924	——
Roots				
Black Spruce 2.0 mm	-2.11	0.04	4868	——
Soil pools (lysimeters)				
Forest floor horizon (~10 cm depth)	-1.03	0.04	7.71	——
Upper B horizon (~35 cm depth)	-0.88	0.04	6.55	——
Extracts and acid leaches (B/C horizon, 50–65 cm depth)				
$BaCl_2$	-0.84	0.03	1445	0.7224
1N HNO3	-0.95	0.03	713	0.7370
15N HNO3	-1.17	0.03	1521	0.7943
residue	——	——	——	0.7176
Plot 2.2				
Foliage				
Black spruce - a	-1.43	0.06	7883	——
Black spruce - b	-1.22	0.04	7841	——
Jack pine	-0.38	0.06	3487	——
Stemwood				
Black spruce - b	-1.81	0.04	1020	——
jack pine	-0.89	0.04	782	——
Roots				
Black Spruce 2.0 mm	-2.20	0.03	3687	——
jack Pine	-1.54	0.04	2145	——
Soil pools (lysimeters)				
Forest floor horizon (~10 cm depth)	-0.83	0.04	3.59	——
Upper B horizon (~35 cm depth)	-0.78	0.07	2.80	——
Extracts and acid leaches (B/C horizon, 50–65 cm depth)				
$BaCl_2$	-0.94	0.03	231	0.7147
1N HNO3	-1.15	0.04	903	0.7363
15N HNO3	-1.16	0.03	1107	0.8229
residue	——	——	——	0.7122
Plot 2.3				
Foliage				
Black spruce - a	-1.28	0.07	10071	——
Black spruce - b	-1.43	0.04	10355	——
Stemwood				
Black spruce - b	-1.65	0.04	1356	——
Soil pools (lysimeters)				
Forest floor horizon (~10 cm depth)	-0.91	0.03	5.63	——
Ah (~20 cm depth)	-0.90	0.03	6.03	——
Upper B horizon (~35 cm depth)	-0.81	0.06	5.90	——
Groundwater				
1.4m	-0.80	0.06	8.39	——
1.8 m	-0.69	0.07	17.14	——
Extracts and acid leaches (B/C horizon, 50–65 cm depth)				
$BaCl_2$	-0.91	0.03	1234	0.7297
1N HNO3	-0.91	0.03	1159	0.7392
15N HNO3	-1.18	0.06	1909	0.7730
residue	——	——	——	0.7150
Other				
Streamwater				
15-Jul	-0.70	0.03	4.81	——
23-Jun	-0.65	0.05	4.38	——
1-Jul	-0.59	0.05	4.22	——
7-Jul	-0.55	0.06	4.55	——
31-Jul	-0.58	0.05	5.48	——
1-Sep	-0.53	0.05	5.07	——
21-Sept	-0.63	0.06	5.65	——
19-Oct	-0.63	0.06	4.70	——
Granite				
Bulk	-1.27	0.04	19022	0.7089
1 N HNO_3 Leach	-1.36	0.05	——	0.7152
15 N HNO_3 Leach	-1.57	0.04	——	0.8950
Corrected for ^{87}Sr growth (Rb = 43 ppm)			——	0.7068
Potted plant				
Basalt	-0.88	0.05	——	——
root (radicle)	-1.30	0.05	——	——
root (secondary)	-1.29	0.06	——	——
stem	-1.38	0.05	——	——
leaf	-0.52	0.08	——	——

1.See Bélanger and Holmden (submitted) for complete $^{87}Sr/^{86}Sr$ dataset

Table 3. Separation factors describing the distributuon of $\delta^{44}Ca$ between trees and soil pools by species

Tree	Plot	Stem	Foliage	Roots	stem-FF[1]	stem-B[2]	stem-B/C[3]	foliage-stem	stem-root
				2.0 mm	——————*separation factors*——————				
t. aspen	1.1	-1.79	-1.30	-2.18	-0.77	-1.00	-0.99	0.49	0.39
t. aspen	1.2	-1.44	-0.96	-2.03	-0.39	-0.75	-0.88	0.48	0.43
t. aspen	1.3	-1.40	-0.89	——	-0.55	-0.85	-0.72	0.51	——
				mean	-0.57	-0.85	-0.86	0.49	0.41
				s.e.	0.11	0.07	0.08	0.01	0.02
j. pine	1.1	-1.14	-0.64	-1.57	-0.12	-0.35	-0.34	0.50	0.43
j. pine	1.2	-1.19	-0.65	n.d.	-0.14	-0.50	-0.63	0.54	——
j. pine	2.2	-0.89	-0.38	——	-0.06	-0.11	0.05	0.51	——
				mean	-0.11	-0.32	-0.31	0.52	0.43
				s.e.	0.02	0.11	0.20	0.01	
b. spruce	1.1	-1.58	-1.20	——	-0.56	-0.79	-0.78	0.38	——
b. spruce	1.2	-1.68	-1.24	-2.11	-0.63	-0.99	-1.12	0.44	0.43
b. spruce	1.3	-1.60	-1.31	0.00	-0.75	-1.05	-0.92	0.29	——
b. spruce[4]	2.1	-1.26	-1.04	——	-0.23	-0.38	-0.42	0.22	——
b. spruce	2.2	-1.81	-1.22	-2.2	-0.98	-1.03	-0.87	0.59	0.39
b. spruce	2.3	-1.65	-1.43		-0.74	-0.75	-0.74	0.22	——
				mean	-0.73	-0.92	-0.89	0.36	0.41
				s.e.	0.16	0.14	0.15	0.14	0.03
Grand mean (spruce and aspen)					-0.67	-0.90	-0.88		
					0.18	0.13	0.13		
Grand mean (all species)								0.43	0.41
								0.12	0.02

1. FF = Ca from FF soil solution collected using lysimeter
2. B = Ca from upepr B soil solution collected using lysimeter
3. B/C = Ca from $BaCl_2$ extract of B/C horizon
4. Plot 2.1 stemwood $\delta^{44}Ca$ not included in averages or grand mean.

Table 4. Ca in soil and vegetation pools and weighted $\delta^{44}Ca$ values

Type	Sampled Depth (cm)	f_u[4] (mol $m^{-2}y^{-1}$)	Ca pools[1] (mol m^{-2})	$\delta^{44}Ca$ (‰)	f_u[4] (mol $m^{-2}y^{-1}$)	Ca pools[1] (mol m^{-2})	$\delta^{44}Ca$ (‰)
Vegetation		**Plot 1.1**			**Plot 2.1**		
Stem[2]			0.832	-1.60		0.92	-1.25
Foliage			0.267	-1.18		0.66	-1.15
Roots[3]			0.197	-1.63		0.22	-1.30
Plot avg. (weighted)		0.0549	1.30	-1.52	0.0939	1.80	-1.22
Soil pools							
Forest floor	10		0.1623	-1.02		1.00	-1.03
Upper B	35		0.1185	-0.79		6.55	-0.88
B/C	50–65			-0.80			-0.84
Vegetation		**Plot 1.2**			**Plot 2.2**		
Stem[2]			1.128	-1.54		0.73	-1.81
Foliage			0.315	-1.20		0.56	-1.33
Roots[3]			0.215	-1.57		0.17	-1.82
Plot avg. (weighted)		0.0808	1.66	-1.48	0.0794	1.45	-1.63
Soil pools							
Forest floor	10		0.8705	-1.05		0.31	-0.83
Upper B	35		0.4840	-0.85		1.47	-0.78
B/C	50–65			-0.56			-0.94
Vegetation		**Plot 1.3**	**Plot 1.3**		**Plot 2.3**		
Stem[2]			0.996	-1.63		1.51	-1.65
Foliage			0.611	-1.32		0.56	-1.36
Roots[3]			0.344	-1.66		0.30	-1.67
Plot avg. (weighted)		0.0873	1.95	-1.54	0.1097	2.38	-1.58
Soil pools							
Forest floor	10		1.228	-0.85		1.52	-0.91
Ah	20		3.202	-0.55		2.61	-0.90
Upper B	35		4.576	-0.45		5.480	-0.81
B/C	50–65			-0.68			-0.91

1. Soil Ca pools based $BaCl_2$ technique. Vegetation pools determined using allometric equations of Lambert et al. (2005).
2. Stem Ca pool consists of stemwood, branches, and bark.
3. Root Ca concentration estimated by method described in Bélanger and Holmden (submitted).
4. Ca uptake flux caclulated as the yearly flux of Ca needed to replace foliage (see text for explanation).

Table 5. Principal inputs and modeled Ca fluxes and fractionation factors for each plot using steady state equations.

Plot	$\Delta_{soil}^{veg\,1}$	X	f_a	δ_{lf}	$\left(\frac{Ca_a}{Ca_a + Ca_w}\right)_{veg}^2$	f_{lf}	f_z	f_w	f_{gw}
	‰		mol m^{-2} y^{-1}	‰		mol m^{-2} y^{-1}	mol m^{-2} y^{-1}	mol m^{-2} y^{-2}	mol m^{-2} y^{-1}
	——————output——————					——output——————			
1.1	-0.611	0.52	0.0180	-1.18	0.94	0.0784	0.0677	0.0016	0.0431
1.2	-0.530	0.50	0.0175	-1.20	0.62	0.1131	0.0904	0.0165	0.0663
1.3	-0.839	0.63	0.0125	-1.32	0.56	0.0865	0.0443	0.0138	0.0255
2.1	-0.239	0.67	0.0185	-1.15	0.91	0.0861	0.0420	0.0043	0.0151
2.2	-0.809	0.78	0.0110	-1.33	0.77	0.0896	0.0391	0.0337	0.0550
2.3	-0.701	0.74	0.0110	-1.36	0.55	0.1168	0.0470	0.0453	0.0634
Average	-0.70	0.64	0.015			0.095	0.055	0.019	0.045
1σ	0.13	0.12	0.003			0.016	0.020	0.017	0.021

1. Average does not include the fractionation factor from plot 2.1.
2. Apportioning of Ca between atmopsheric deposition and soil mineral weathering sources in vegetation using $^{87}Sr/^{86}Sr$ as a tracer (Bélanger and Holmden, submitted).

Figure 1


60°
Taiga
Shield
Cree Lake
Boreal
Shield
Study area
Nemeiben L.
La Ronge
Lac La
Ronge
Prince Albert
National Park
Candle L.
Boreal
Plain
Prince Albert
Saskatoon
Wynyard
Kindersley
Regina
Prairie
Province of Saskatchewan
49°

Fig.2
Holmden and Bélanger

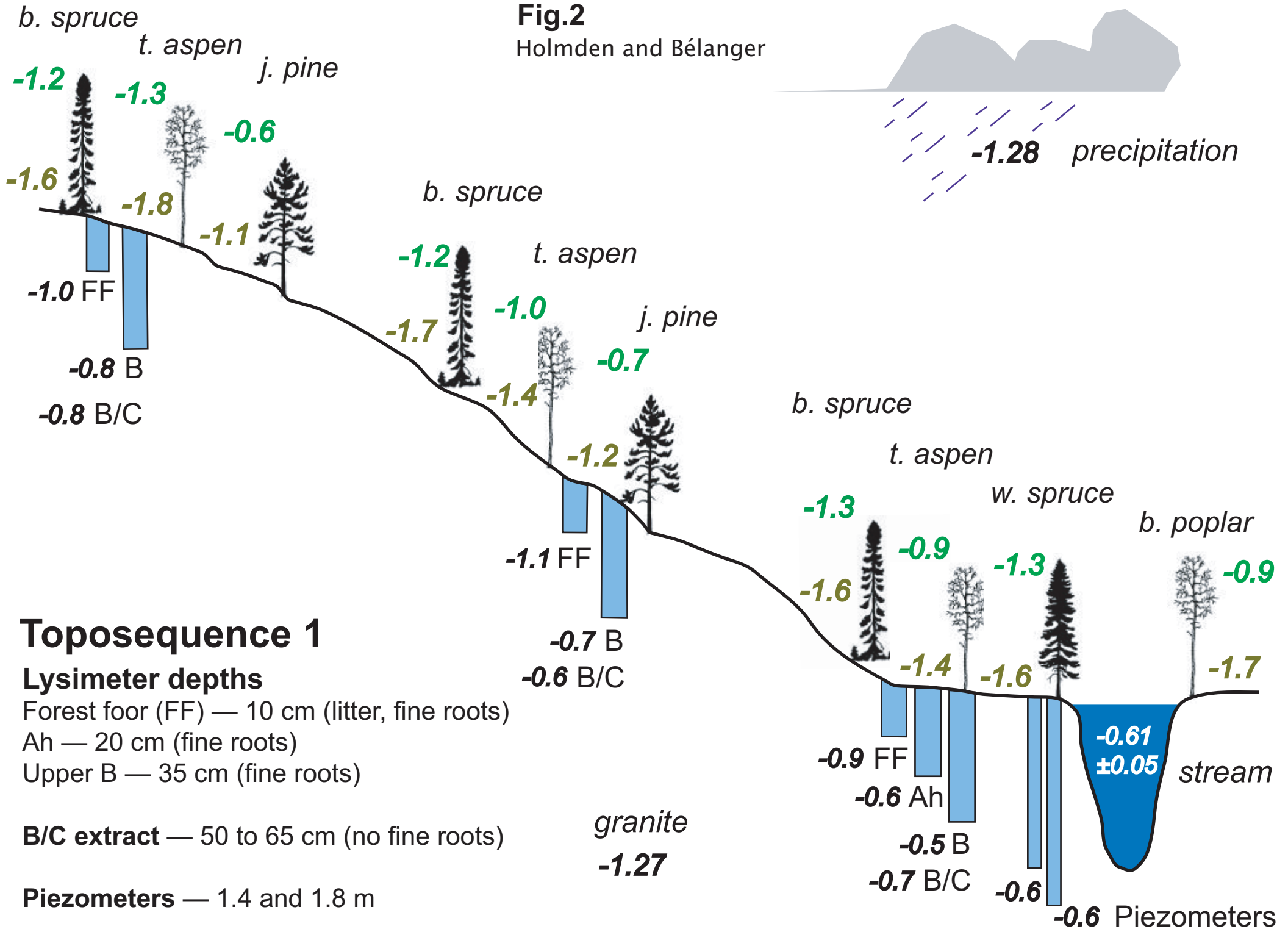

Toposequence 1

Lysimeter depths
Forest foor (FF) — 10 cm (litter, fine roots)
Ah — 20 cm (fine roots)
Upper B — 35 cm (fine roots)

B/C extract — 50 to 65 cm (no fine roots)

Piezometers — 1.4 and 1.8 m

Plot 1.1 sand	Plot 1.2 loamy sand	Plot 1.3 silty clay	

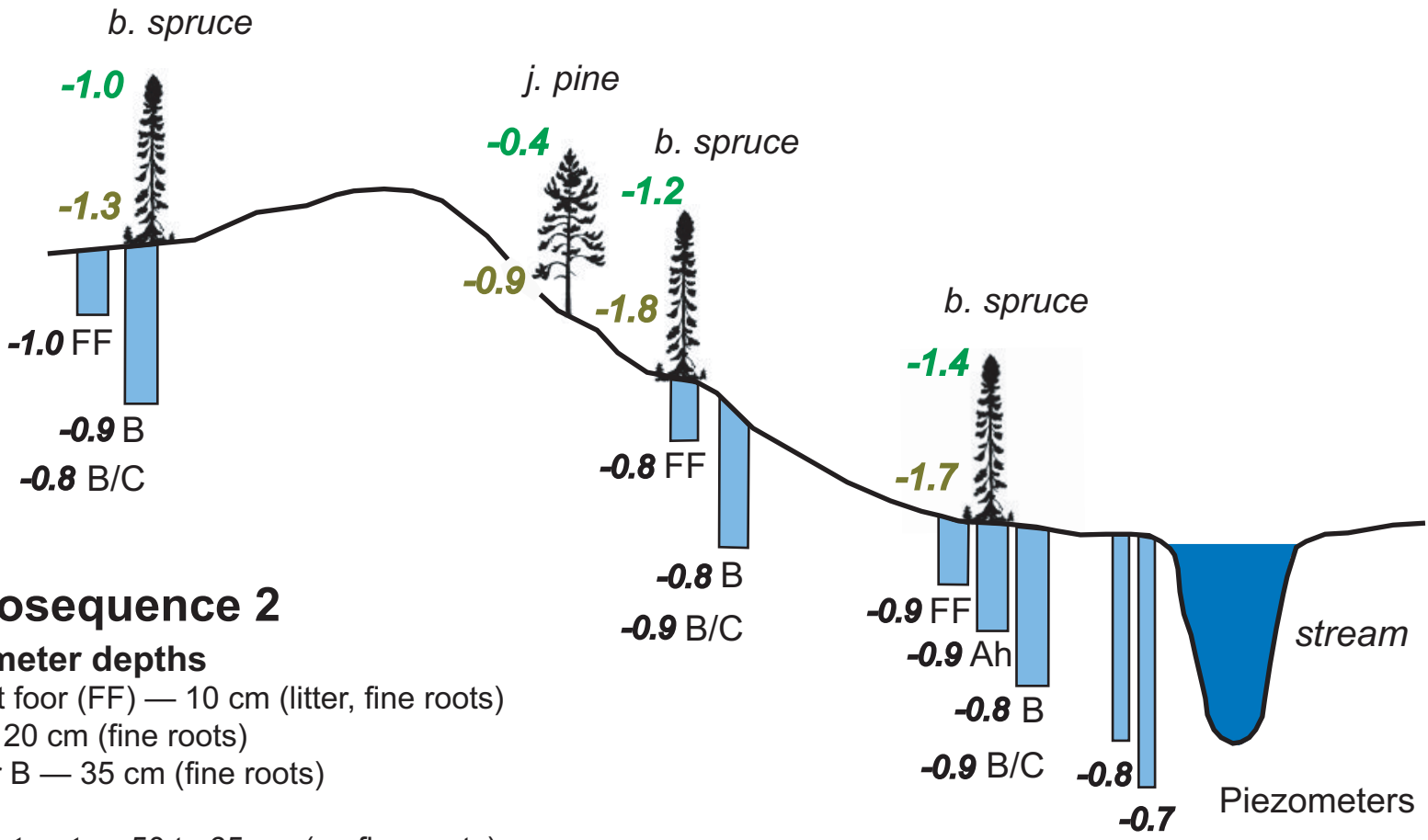

Toposequence 2

Lysimeter depths

Forest foor (FF) — 10 cm (litter, fine roots)
Ah — 20 cm (fine roots)
Upper B — 35 cm (fine roots)

B/C extract — 50 to 65 cm (no fine roots)

Piezometers — 1.4 and 1.8 m

Plot 2.1 silty clay	Plot 2.2 loamy sand	Plot 2.3 silty clay	

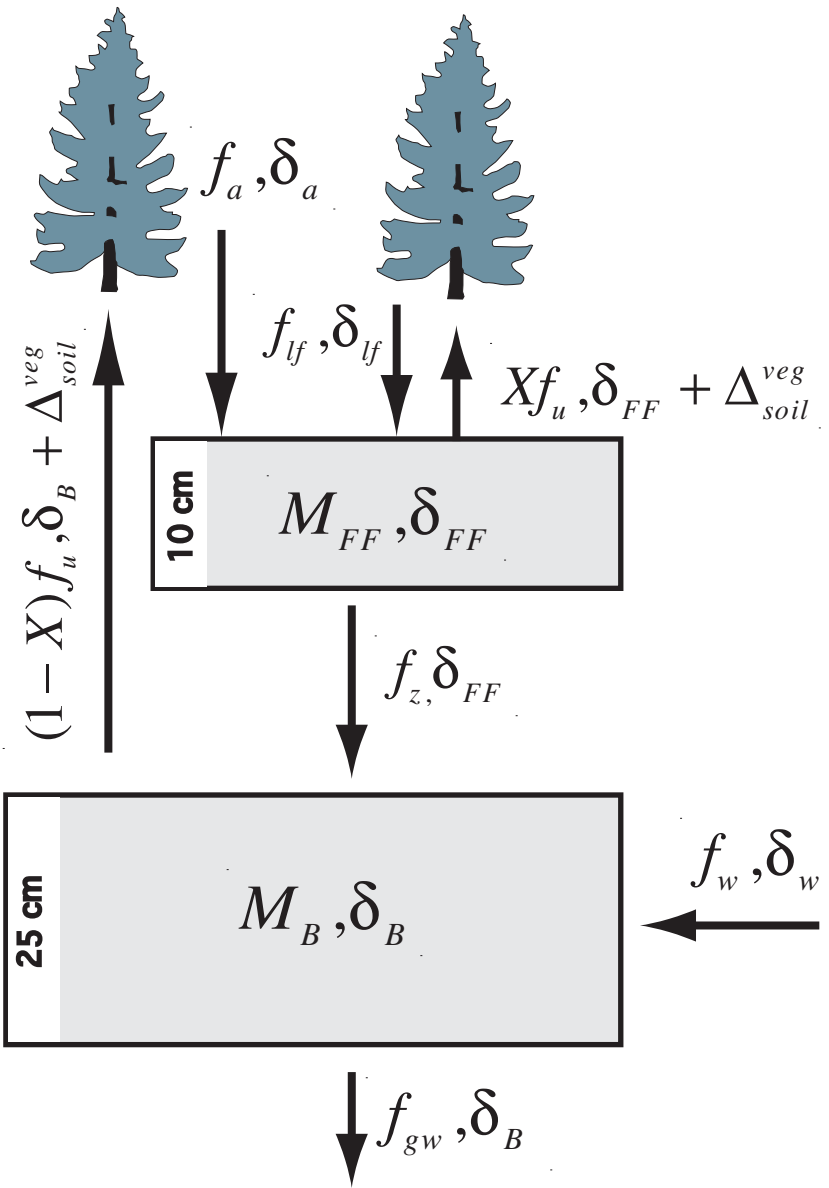
f_a, δ_a
f_{lf}, δ_{lf}
$Xf_u, \delta_{FF} + \Delta^{veg}_{soil}$
$(1-X)f_u, \delta_B + \Delta^{veg}_{soil}$
10 cm
M_{FF}, δ_{FF}
f_z, δ_{FF}
25 cm
M_B, δ_B
f_w, δ_w
f_{gw}, δ_B

Fig. 5

Holmden and Bélanger

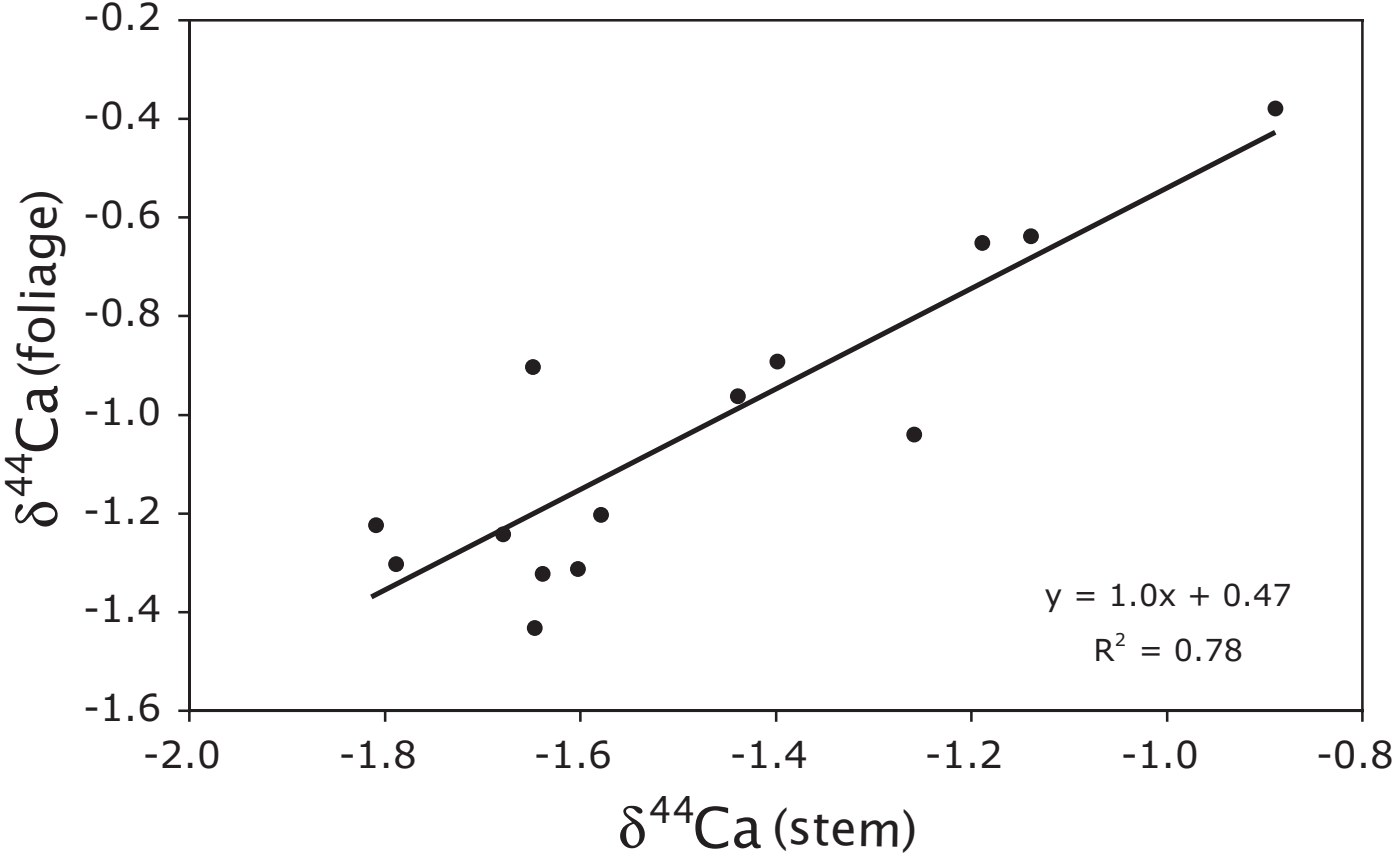

Fig. 6 Holmden and Bélanger

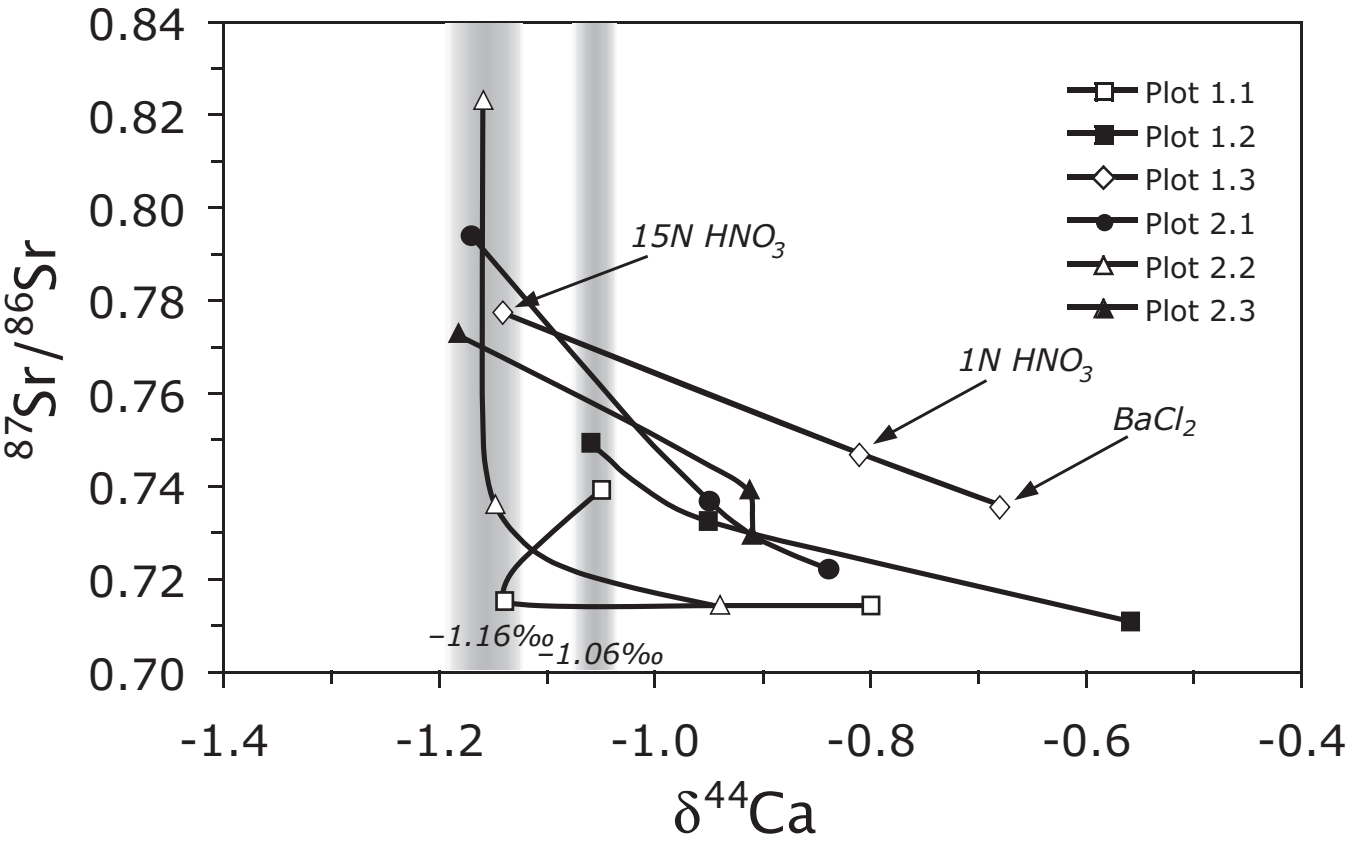

Fig. 7

Holmden and Bélanger

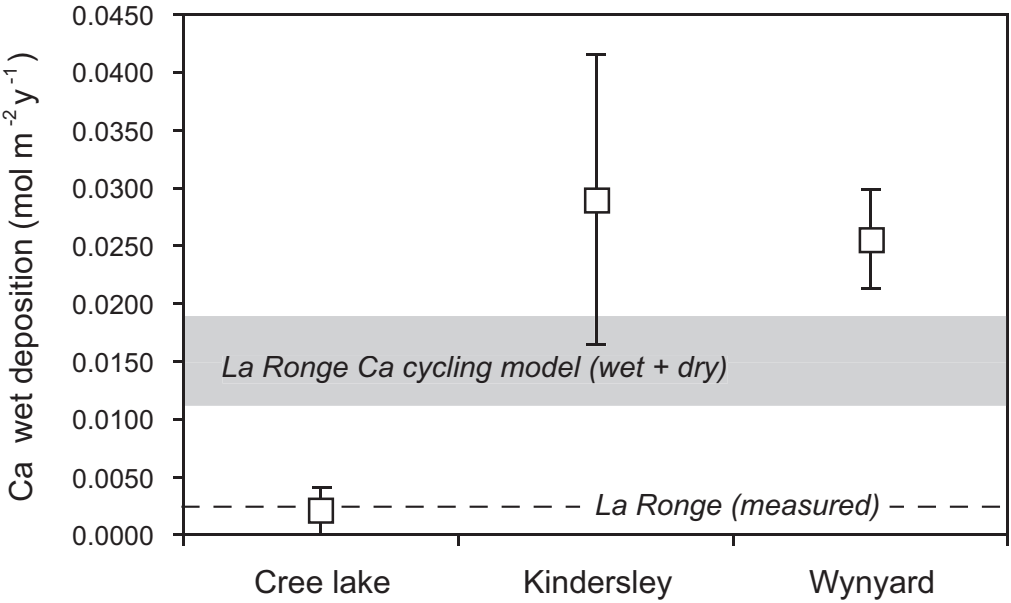

Fig. 8 Holmden and Bélanger

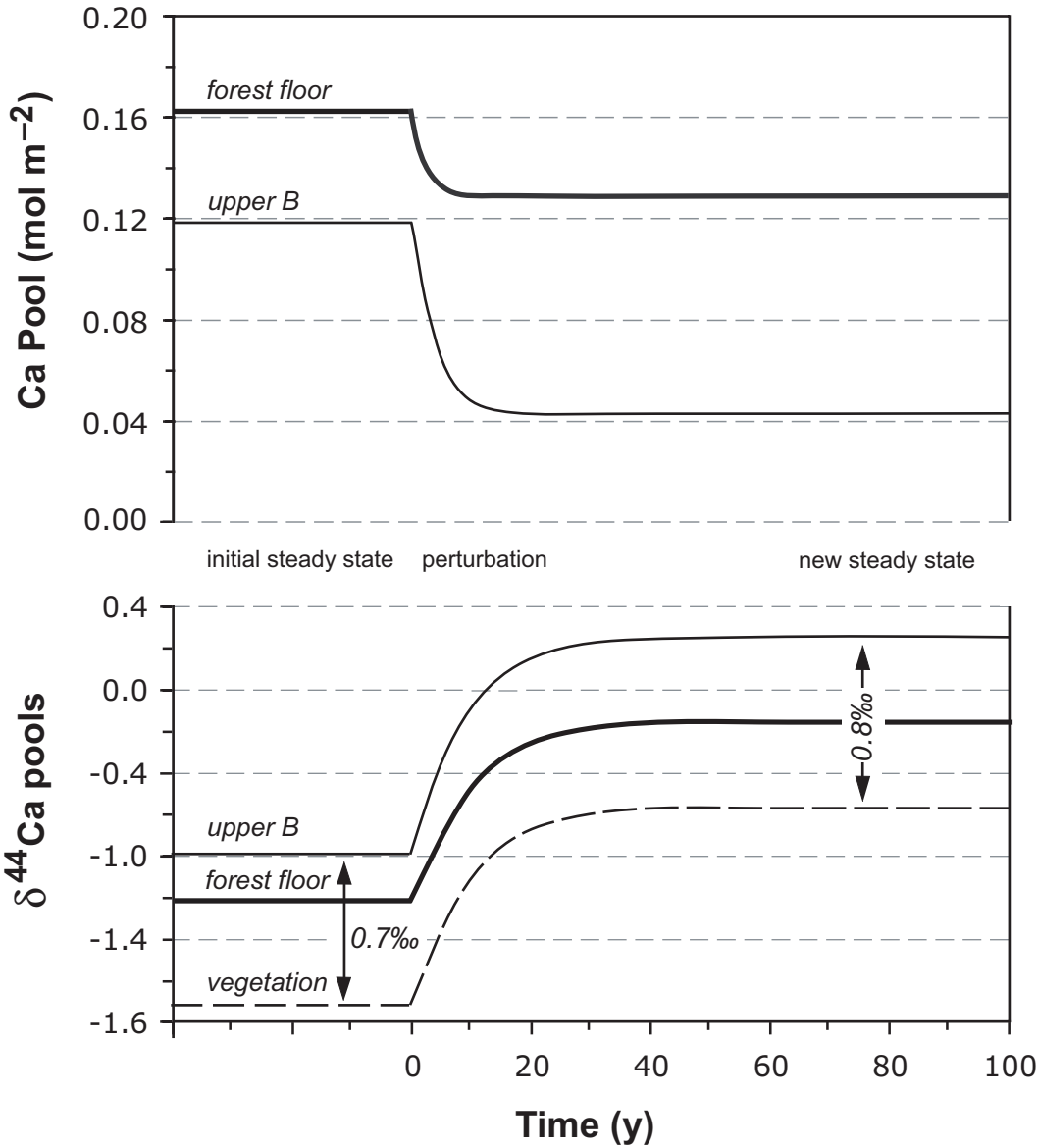

Fig. 9

Holmden and Bélanger

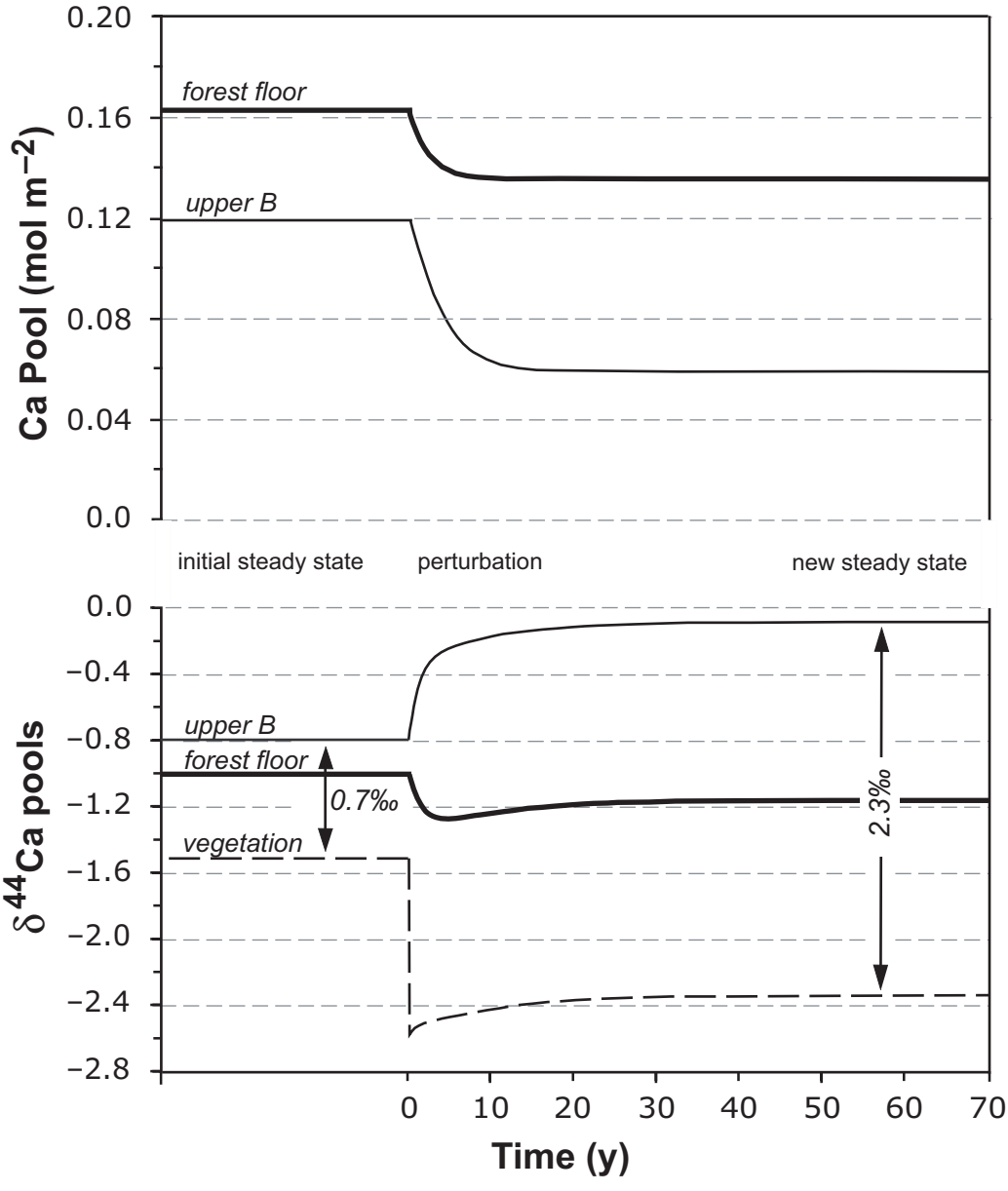

Fig. 10 Holmden and Bélanger

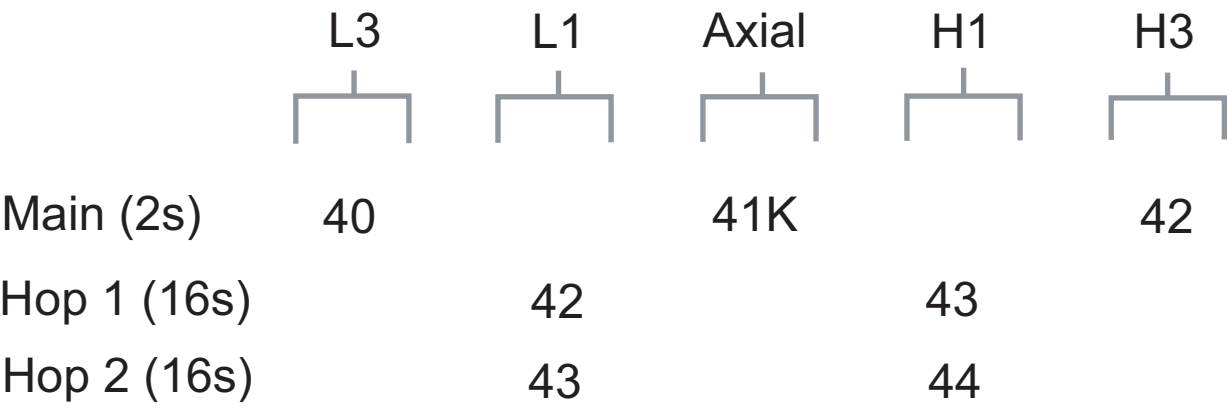

Fig. 11

Holmden and Bélanger

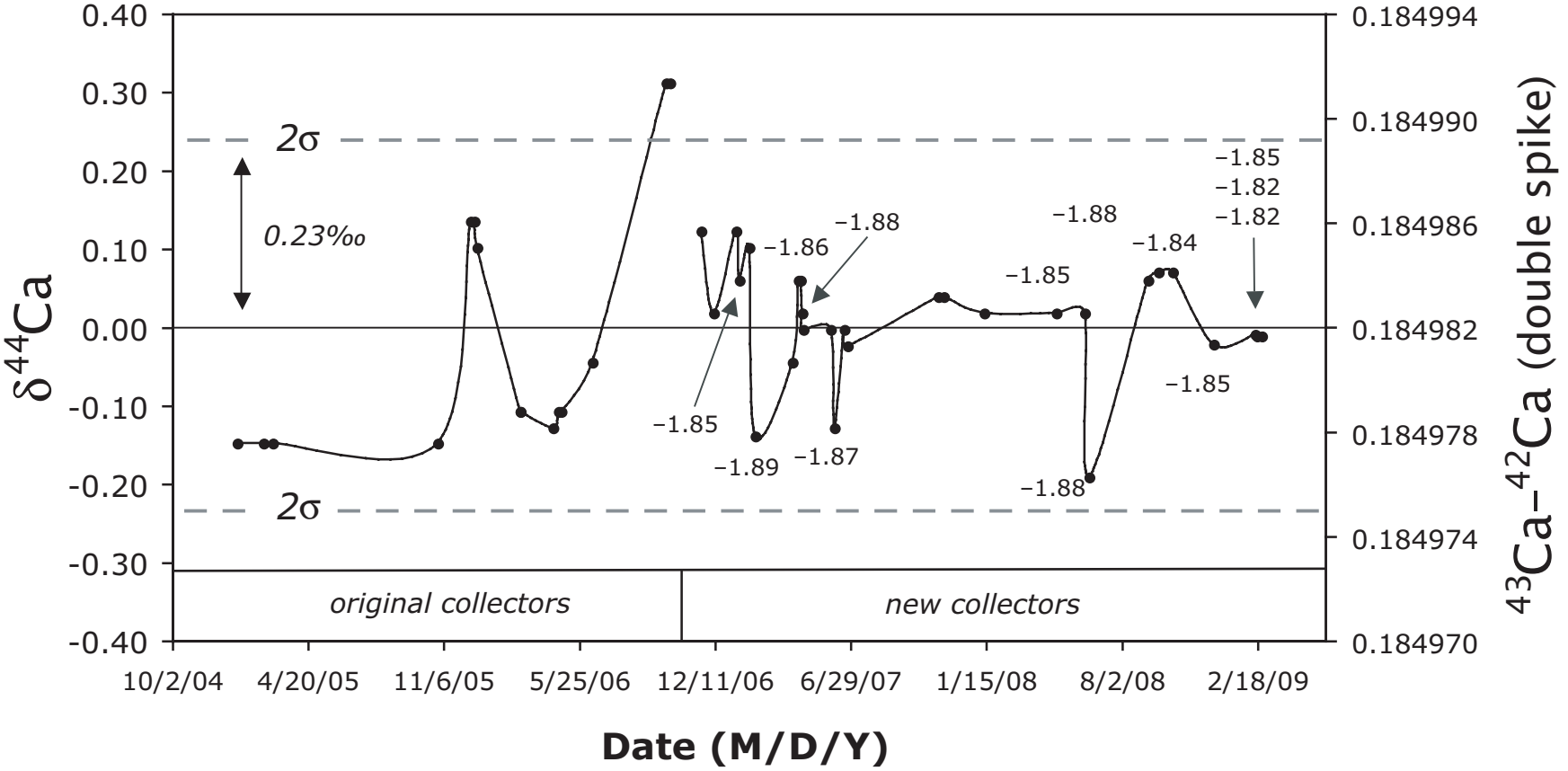

Fig. 12

Holmden and Bélanger

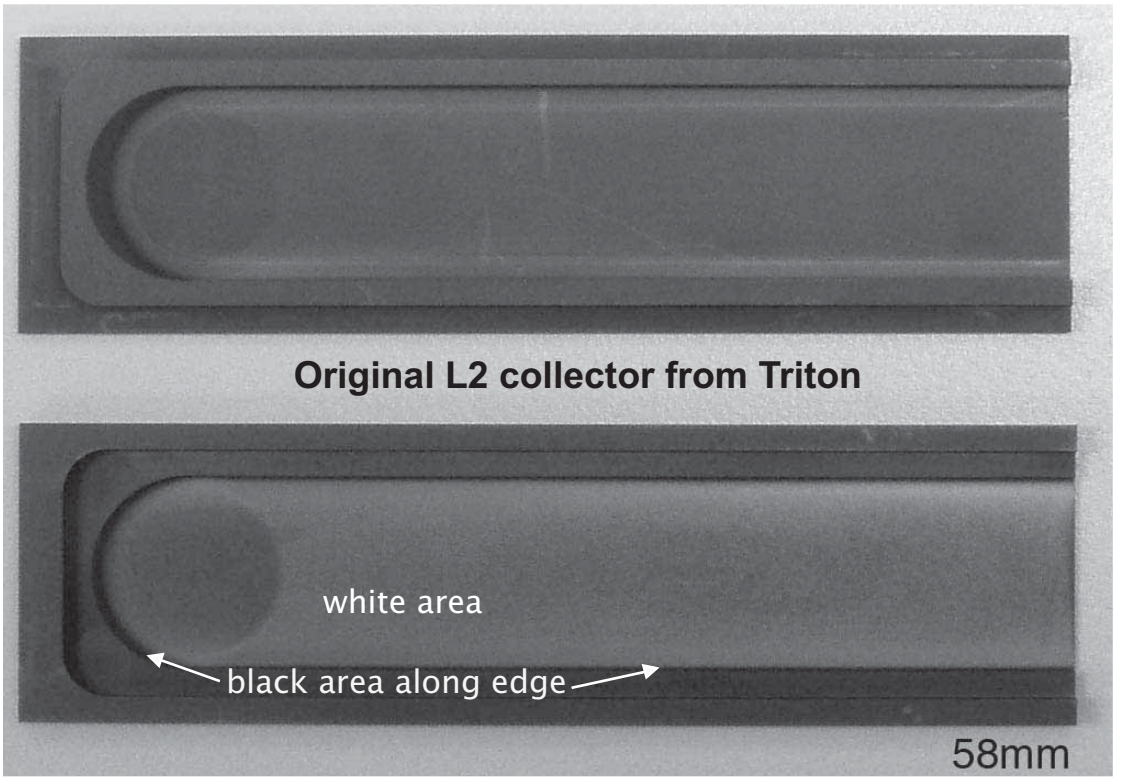

Fig. 13

Holmden and Bélanger